McGill University

Masters Thesis

Design and application of combined AFM-SICM for the investigation of lithium charging events

Authour:
Tyler Leslie Brian Enright

Supervisor:
Dr. Peter Grütter

A thesis submitted in partial fulfillment of the requirements of the degree of Master of Science

in the

Physics Department
McGill University, Montreal

August 2014

Abstract

Viability of tips for use in an integrated Scanning Ion Conductance Microscopy and Atomic Force Microscopy (SICM-AFM) system intended for study of lithium ion battery charging characteristics was examined and many probes were fabricated. Capillary tubes and x-ray diffraction tubes were bent by voltaic arc to demonstrate that hollow pipettes could be formed into the shape of AFM cantilevers to be used within the Electrochemical Atomic Force Microscope. The probes were coated with aluminum for reflectivity and were mounted on silicon chips on the AFM head optical rod for stability. Probes of 5mm in length were made and tested. A resonance of 4545Hz was found, which was close to the value calculated from geometric and physical parameters of 4095Hz. Polishing a flat surface on the probes failed to increase reflectivity but an aluminum coated glass reflector mounted on a probe increased the reflected signal by an order of magnitude. AFM scans of DVD pits were performed where in the first few scans the probes resolution was better than 160nm, but quickly decreased to close to 300nm. The tips were examined by Scanning Electron Microscopy (SEM) and it was hypothesized that small unstable features on the tip end surface were responsible for the high resolution. The ability of these tips to perform high resolution measurements initially, the non-uniform but open tips created by the voltaic arc tapering method, and the large amplitude damping of the probe in water suggests that while pipette cantilevers can be used for topography and this probe geometry can probably be used for SICM measurements, x-ray diffraction tubes pipettes pulling isn't capable of sharp enough tips. Using a pipette puller, pipettes with a tip size of an estimated 30nm, widening to approximately $10\mu m$ for a length of $400\mu m$ were created. Calculations predict that the probes' resonance frequencies and stiffness constants will be similar to that of the x-ray diffraction tube probes, but the decreased tip size indicates resolution on the order of 30nm. This work lays the groundwork for an integrated SICM-AFM system of high spatial and current resolution.

Résumé

La viabilité de différentes pointes pour usage dans un système intégré de "Scanning Ion Conductance Microscopy" (SICM) et de microscopie à force atomique (MFA) destiné à l'étude des caractéristiques de chargement des batteries lithium-ion est évaluée et plusieurs sondes sont fabriquées. Des tubes capillaires et des tubes pour diffraction de rayons x sont pliés par un arc électrique pour démontrer que des tubes ouverts peuvent être remodelées dans la forme d'un cantilever de MFA pour être utilisées dans un MFA électrochimique. Des sondes faites à partir de tubes pour diffraction de rayons x ont été recouvertes d'une couche d'aluminium pour les rendre réfléchissantes et ont été fixées sur des supports de silicium à la tête de la tige optique d'un MFA pour en assurer la stabilité. Des sondes d'une longueur de 5mm ont été fabriquées et testées. Une fréquence de résonance de 4545Hz a été mesurée ce qui est près de la valeur théorique de 4095Hz calculée à partir des paramètres géométriques et physiques de la sonde. Le polissage de la sonde pour en aplanir la surface n'a pas augmenté sa réflectivité mais en plaçant un réflecteur de verre enduit d'aluminium sur la sonde, l'intensité du signal réfléchi a augmentée par un ordre de grandeur. Des images de MFA des fossés à la surface d'un DVD sont obtenues dans lesquelles la résolution de la sonde est estimée meilleure que 160nm mais celle-ci dégrade rapidement autour de 300nm. Les pointes sont examinées par microscopie électronique à balayage et les résultats suggèrent que des petites bosses instables sur la surface de la pointe déterminent la résolution obtenue. La capacité qu'ont ces pointes de réaliser des mesures à relativement haute résolution ainsi que la présence d'une ouverture à la pointe créée par la méthode de dégression en utilisant un arc électrique suggère que les cantilevers faits à partir de tubes peuvent être utilisés pour faire des mesures de MFA et que leur géométrie est adéquate pour faire des mesures de SICM. Toutefois, les sondes faites à partir de tubes pour diffraction de rayons x ne produisent pas des pointes assez fines et la sonde subit un amortissement d'amplitude dans l'eau. En utilisant un tire-pipette, des tube capillaires avec une pointe d'une taille d'environ 30nm s'élargissant jusqu'à $10\mu m$ pour une longueur de $400\mu m$ sont fabriquées. Des calculs prédisent que la fréquence de résonance et la constante de rappel de ces sondes seraient similaires à celles de sondes faites à partir de tubes pour diffraction de rayons x à l'avantage que la petite taille de leur pointe permettraient une résolution de l'ordre de 30nm. Ce travail établit donc la base pour un système intégré de SICM-MFA à haute résolution spatiale et de courant.

Acknowledgements

Thanks to Peter Grütter for supervising this project and guiding its development as well as my understanding of AFM and scientific scholarship in its totality.

Yoichi Miyahara's vast knowledge of electronics and AFM, and the advice produced therein has been indispensable.

Aleks Labuda's contribution of design and creation of the Electrochemical Atomic Force Microscope which I use, and the design of the AFM head made specifically for this project, has been essential to any success of this project, and is greatly appreciated.

Aaron Mascaro's partnership in working on AFM and understanding the topics related to lithium batteries has helped accelerate my own work and understanding.

Sankha Mukherjee's COMSOL modeling of the initial SICM-AFM probe was a great boon in directing the initial probe creation.

Monserratt Lopez's knowledge of pipette pulling and SNOM probe creation has helped greatly in development of the probes.

Contents

Chapter 1

Motivation

1.1 Batteries

In the broadest terms, the goal of this project is to develop a technique that will allow for the study and improvement of battery materials. Battery materials and technologies, while important in current technologies, will play an increasingly important role in the coming years. In fact by 2020 it is expected that the worldwide electrical energy storage market for automotive vehicles alone will exceed $37 billion [1].To be competitive in such a lucrative market battery materials are being sought to fulfill three main criteria: high energy density, high power capability and long lifetime durability. The most prominent issues of the current energy storage climate demonstrate clearly why these are important characteristics.

1.1.1 Grid Energy Storage

During a daily cycle, energy provided by the grid is not used at a consistent rate. This can be explained simply by the needs of the individual customers changing throughout the day. Examples include the population's eating times, sleeping times, and the times at which lights are used on a given day. This means that a system which provides uniform energy throughout a given day will either provide excess energy or demand energy that the system cannot provide periodically throughout the day. One might think that predicting and reacting to these energy demand changes may be accomplished by changes in the amount of energy generated. While this is true, continuously increasing and decreasing

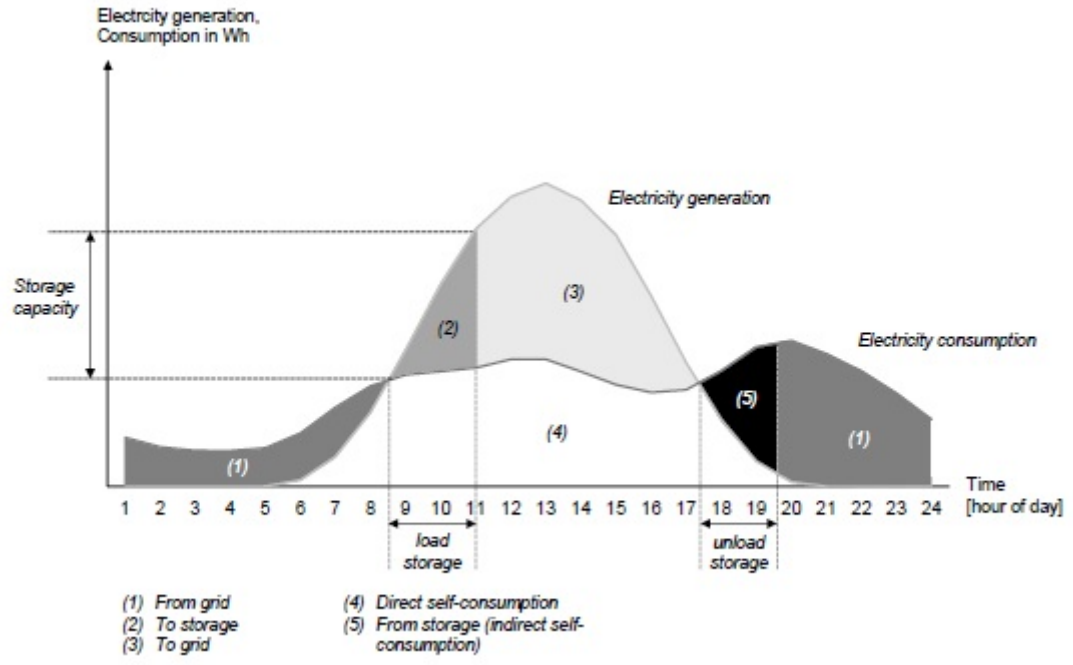

FIGURE 1.1: General logic of self-consumption calculation module (illustrative) [2]

the rate of energy generation within the system is a huge source of inefficiency and wear on the system. As shown in figure 1.1, changes in energy demand are large and occur rapidly [2]. In fact, not only does the energy demand change during the day, but due to the weather and season dependent nature of most renewable energy sources, the supply of energy is also quite variable. The energy supplied by these renewable energy sources cannot be artificially increased, thereby limiting their use in adjusting to increases in energy demand.

A logical choice in dealing with varying energy demands is to create a system which may dynamically adjust to energy needs by storing energy during times when production exceeds demand, and releasing that stored energy when demand exceeds production. This is what is referred to as grid energy storage.

The method of pumped-storage hydroelectricity (pumped hydro) consists of transporting large volumes of water, and using the change in potential energy as storage of energy. Through use of a reversible turbine, water energy may be used to pump water into a reservoir. This reservoir is pumped above the initial pool of water, so that by elevating water into the reservoir gravitational energy is gained. When the stored energy is needed by the grid, water is drained from the reservoir, which powers a turbine, converting the gravitational energy of the water to electrical energy. There are significant losses during

these operations however. Due to mechanical inefficiencies and evaporation of the exposed water reservoirs it is estimated that 70% to 75% of stored electrical energy is recovered when converted back to electrical energy [3]. On top of this, there are large issues with the storage volume incurred. In order to store large amounts of energy, the volume of water stored in a given reservoir must be proportionally large. This may mean the creation of a dam, and the creation of a large artificial water source which may flood the surrounding area, which may result in environmental destruction.

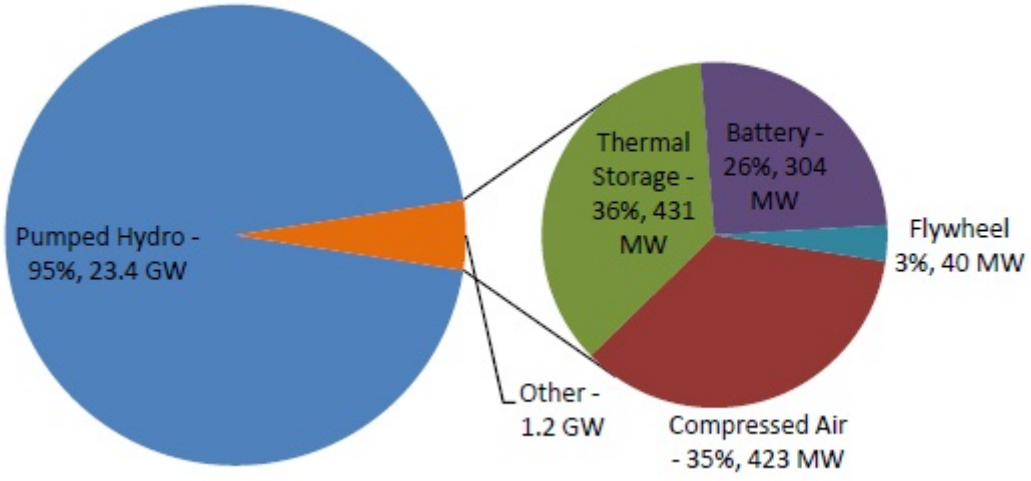

FIGURE 1.2: Rated power of U.S. grid storage projects (includes announced projects) [2]

Currently, pumped hydro accounts for roughly 95% of the U.S. grid storage, and 99% of power storage worldwide [4]. As shown in figure 1.2, battery storage accounts for 26% of the remaining 5% of grid storage in the U.S. If battery storage is to compete as a grid level storage option, then it must be shown to outperform the pumped hydro in some key areas.

As shown in figure 1.3, one key area in which lithium-ion batteries outperform pumped hydro is discharge time [5]. If grid storage changes are predictable, pumped hydro is an attractive option due to it's low cost. However, the rapidly changing output of renewable energy sources, and the sudden demand incurred during power system failures (for example, hail storms disrupting power lines) require immediate response. Certain services, such as hospitals, cannot afford to wait for the longer response times of pumped hydro. Batteries must also be able to compete via physical characteristics. In terms of efficiency,

lithium-ion technology already has the edge with an estimated 90-94% efficiency [6]. However, pumped hydro can be discharged at less than 100 $/kWh [7], whereas the cost when using lithium-ion batteries is 900-1700 $/kWh [6]. To reduce the cost of lithium-ion batteries lifetime durability must be increased. As of 2011 lithium-ion batteries in grid storage devices had an average lifetime of 4500 cycles with a discharge duration of 2-4 hours[6]. If we accept that these batteries are being continuously cycled this equates to less than two years of working life. It can be assumed that these batteries will not be continuously cycled, however a system lifetime on the order of years instead of decades is a major issue that must be addressed before it assumes a more substantial role in large scale energy grid storage.

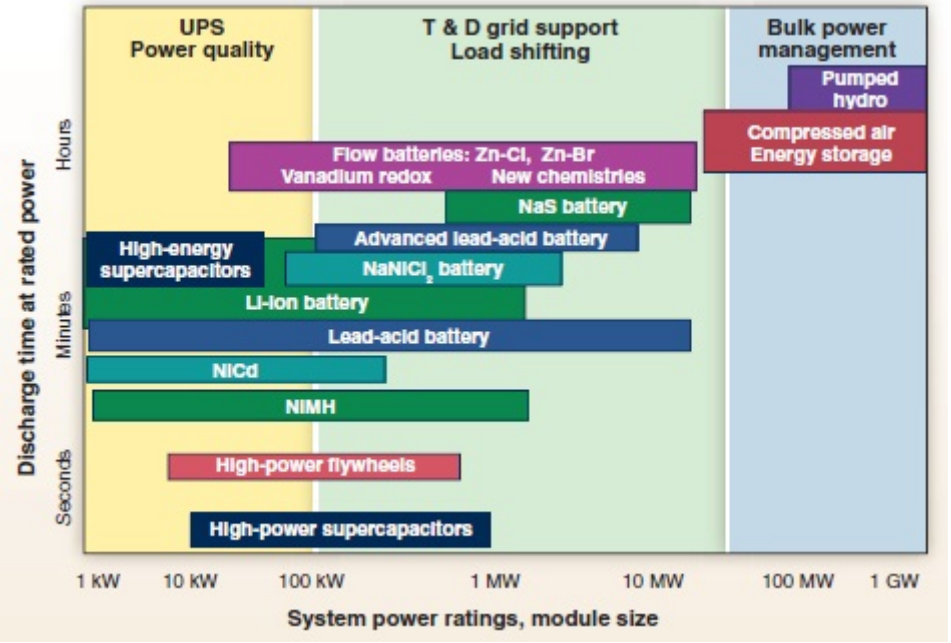

FIGURE 1.3: "Comparison of discharge time and power rating for various electrical energy storage technologies. The comparisons are of a general nature because several of the technologies have broader power ratings longer discharge times than illustrated." [5]

1.1.2 Electric Cars

Hybrid cars are currently a viable option for consumers yet there is still a large push within the energy community to develop fully electric vehicles. By switching to fully electric vehicles it is hoped that the demand on fossil fuels such as petroleum can be drastically reduced. Instead of powering vehicles via fuels which are known to create large amounts of greenhouse gases and other harmful pollution, cars may be fueled by

a

Modes of operation	battery capacity needed, kWh	Energy density, Wh/kg	Weight of battery, Kg	Speed, kilometres per hour	Distance on one charge, kilometres
 Hybrid	<3	40-50 (Ni-MH)	60 (Ni-MH)	100+	15
 Plug in Hybrid	5.6-18	90-100 (Li-ion)	60-200 (Li-ion)	100+	10-60
 Full EV	35-54	90-100 (Li-ion)	450 (Li-ion)	>100	150-200

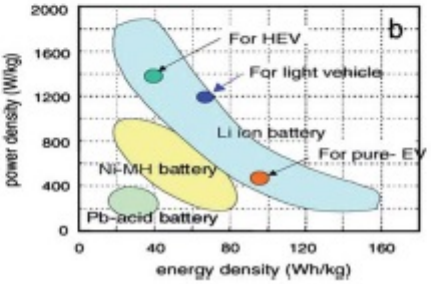

FIGURE 1.4: (a) Characterization of the main three kinds of Electric Vehicles (EV) in terms of performance and battery properties (b) Ragone plot which compares the performance of battery technologies in their currently established ranges of power density and energy density [8]

renewable energy sources which are connected to the grid energy system. Also, in areas which rely on fossil fuels such as coal to power their energy grid, by centralizing energy conversion processes it is hoped that efficiency can be increased. This may only happen if lithium-ion batteries can be produced which are of sufficient efficiency.

Shown in figure 1.4 are the required attributes for each level of more electrically reliant vehicle [8]. The included Ragone plot shows the current capabilities of the leading commercial batteries. Currently, hybrid cars are becoming more prevalent, and the market is beginning to provide fully electric vehicles. To reduce the price of these fully electric cars, energy capacity and energy density must increase. Due to the low operating voltage of lithium-ion batteries at 3.4 Volts the energy density is in turn low at 90-100 Wh/kg [8]. Consumers currently expect to be able to travel approximately 500km on a single tank of gas. Current electric vehicles may travel around 150km on a single charge, which is a major issues for consumers [9]. At first, it would seem that a reasonable solution would be to increase the amount of active battery material in these vehicles. However,

these vehicles must also transport the increased mass of battery material. This means that increases in distance per charge is accompanied with a decrease in vehicle efficiency. Higher density could increase range without decrease in range.

Chapter 2

Background information and theory

2.1 Issues in Battery Material Study

2.1.1 General Model of Lithium Iron Phosphate

In an electrochemical cell, chemical energy is converted to electrical energy by an electrochemical reaction. Lithium ion batteries are charged by applying a current from the positive electrode (anode) to the negative electrode (cathode). By doing so lithium moves from the anode (constituted of iron phosphate) to the cathode (usually graphite). Once the battery is charged there is a potential difference between the cathode and anode. When allowed to discharge the opposite action occurs, and produces a current which may be used to power a connected device.

The actual makeup for the cell consists of this basic scheme. To increase electrical conductivity, the active lithium iron phosphate material is synthesized as a powder of nanoparticles. The small particle size maximizes the ratio of surface area to volume, which is theorized to increase the exposure of active material to the electrolyte, which should increase conductivity of the system [10].

The goal of much of battery electrochemistry is to understand how lithium enters (lithiation) and exits (delithiation) the anode and cathode. The slow rate of lithium ion diffusion, and the low electronic conductivity of lithium iron phosphate present challenges which have been mitigated by carbon binder but remain as barriers to battery performance [11]. The primary aim of my project is the anode material. When the anode

is lithiated, the electrochemistry of this electrode actually changes. The most common model for treating lithium ion batteries was developed by Newman who used combined

> 'porous electrode theory, concentrated solution theory, Ohm's law, kinetic relationships, and charge and material balances [12]'

to describe charging dynamics.

The Porous electrode theory is applied due to the assumption that the electrode consists of a mix of conducting and nonconducting materials mixed together with the active material with an arbitrary geometry in a space with many gaps between materials. As such there are many different localized reaction rates dependent on the many geometrical arrangements within the material. This is then treated as a superposition of interacting materials in the theory.

Concentrated solution theory relates driving forces within the system, like chemical potential, to the mass flux. This keeps to account for transient change in concentration caused by mass flux and reactions.

Ohm's law is used to relate the potential drop over the electrode and electrolyte due to the resistance of each. Furthermore, diffusion potential is taken into account here to explain changes in resistance.

Kinetic relationships, charge balances, and material balances are taken into described by the Butler-Volmer equation where differences in potential between the electrode and solution are related to rates of electrochemical reaction.

The Newman framework is used to predict the quantitative characteristics of the materials, but also makes a key prediction as to the form of intercalation. According to Newman theory, the nanoparticles will be intercalated in a 'shrinking core' model, as shown in figure 2.1 [13]. As the Ceder group as shown through atomistic simulations lithium transport is by far the fastest in the 1D channels of Li_xFePO_4 [14], and so lithium transport will occur through these channels. According to Newman this transport results in a two phase state of fully lithiated and fully delithiated regions where the lithiated regions nucleating on the outer surface of the nanoparticles, and the material being intercalated inwards.

Although the Newman model continues to be used for calculating electrochemical properties, it has been shown experimentally that lithium iron phophate seems to have a different lithiation pattern. The alternative 'domino cascade model' states that, as in

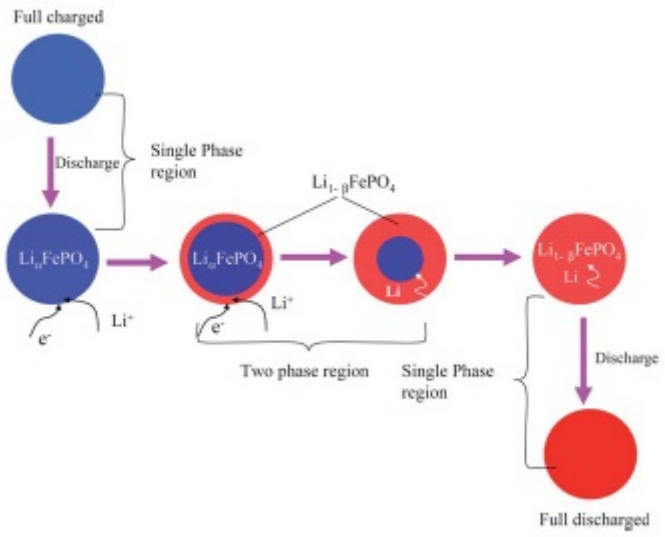

FIGURE 2.1: "Illustration of the shrinking-core model with the juxtaposition of the two phases and the movement of the phase boundary. The processes during discharge are illustrated. Both the single-phase and the two-phase regions are shown."[13]

the Newman model, particles exist as fully intercalated or fully deintercalated. From x-ray diffraction and electron microscopy measurements it has been demonstrated that the minimization of the elastic energy occurs via a wave of intercalation occuring throughout the crystal as shown in figure 2.2 and [15]. Here there is no shrinking core, but a phase boundary aligned with the $FePO_4$ planes, moving perpendicular to the lithium flux.

Although these models are among the most used, they are far from validated, and have even been shown to be incorrect in some measurements. For these models to be verified much more experimental evidence is required.

Furthermore, much of the field of battery development is reliant on progressive modifications of battery synthesis process and basic electrochemical cycling as testing. With a more rigorous understanding of the battery charging process batteries may be designed intelligently and take full advantage of the elementary processes which contribute to high power density and energy density. This will lead to much more efficient and faster battery material development.

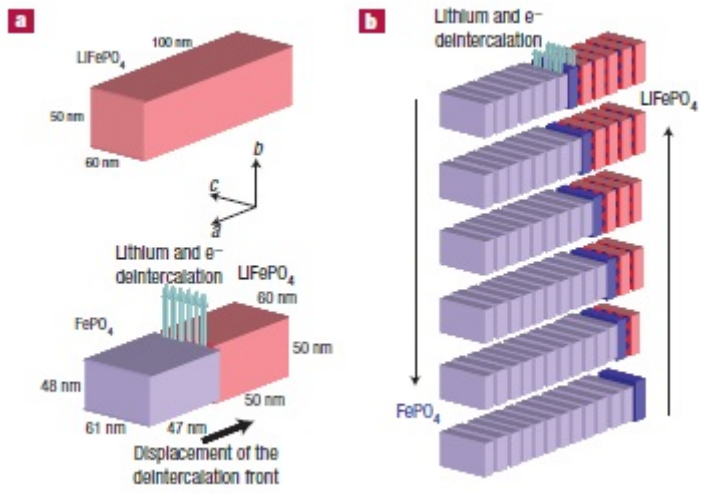

FIGURE 2.2: "Schematic view of the 'domino-cascade' mechanism for the lithium deintercalation/intercalation mechanism in a $LiFePO_4$ crystallite. Distances are not accurate because studied crystallites are rather isotropic. a, Scheme showing a view of the strains occurring during lithium deintercalation. b, Layered view of the lithium deintercalation/intercalation mechanism in a crystallite" [15]

2.1.2 Validation Required of the Current Model

There has been an abundance of theoretical models which aim to describe these mechanisms, although experimental work to validate the assertions of this work has been more sparse. The Newman model is one of the most used frameworks for theoretical study of these batteries. Though there has been experimental work demonstrating that the shrinking core model it predicts does not occur in lithium iron phosphate [15] [16], the Newman model continues to be used to describe battery activity [17].

There is also some controversy over the veracity of this model for use in determining battery characteristics. There is no microstructural information needed beyond particle radius, electrode thickness, and electrode porosity. It assumes that the microstructure can be described as isotropic, homogeneous, one dimensional porous material made up of monodisperse non-porous isotropic spherical particles that are small compared to the electrode thickness [17]. These assumptions cannot be correct however. The charge transfer step assumes a one step global process. However, the charge transfer step in a battery consists of the lithium de-solvating, transported through a surface electrolyte interface which not only consists of electrolyte and active material but of unintended products of side reactions as well, and then react with the electrode. The binder itself is simply absorbed into the parameters of the model rather than by being treated as a

separate entity. To take the entire pathway as one step is to make a large simplifying assumption which ignores the geometries and chemical variation throughout the path of the lithium ions. Furthermore, these steps occur at an atomic level, and atomically inhomogeneities in the battery materials have shown to exist. The geometry at this level is ignored in the model, in fact nearly all geometry is ignored in the Newman approach. The Butler-Volmer step describes how an electrode's electrical current depends on the electrode potential; it describes the electrical charge transfer. It is theorized to have a large part in degradation of the battery materials[17]. These cell degradation processes are poorly defined. One suggestion has been that 'carbon retreat', relating to the carbon binder, has led to the loss of internal electrical conductivity witnessed experimentally. This loss has also been explained by particle fracture, precipitation of thick films at the the surface-electrolyte interphase, gas generation, loss of contact between the current collector and the housing, and loss of contact between the active material and the current collector. However, these issues are quite difficult to measure in situ, so the chain of cause and effect is not quite clear, and atomic reasons for these issues lack a basis that can be strongly integrated into current theory.

Even the domino-cascade model which was thought to have displaced the shrinking-core model has been proven inaccurate [16]. In Ramana's study he has shown through use of x-ray and electron microscopy that dependent on the synthesis technique used to create the lithium iron phosphate sample, the phase boundaries will take on different shapes. That is to say both delithiated and lithiated states may exist within one particle. This leads to much different dynamics, the result being a lithiation scheme which is shown visually in figure 2.3 [18].This has been validated by other studies which claim otherwise, but these studies use different synthesis processes which may affect the lithiation process [19].

Thus, while current theory explains some electrochemical quantities, many details at an atomic level are missing to describe the fundamental interactions within batteries. These fundamental processes are crucial to understanding degradation processes as well as the general process of lithium intercalation, and may only be completely described by a versatile tool which may directly observe lithiation in situ.

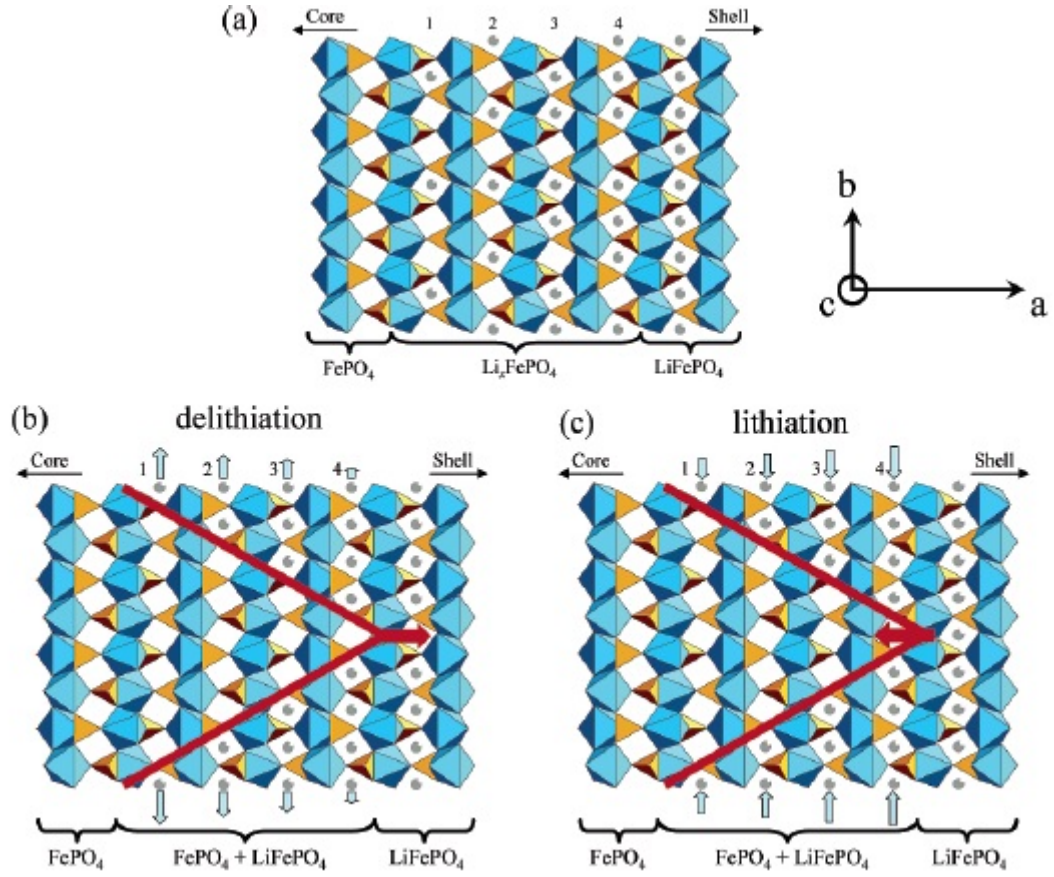

FIGURE 2.3: "Schematic views of the interfacial region between $LiFePO_4$ and $FePO_4$ phases. (a) Hypothesis of a disordered LixFePO4 phase with a gradient of Li content between FePO4 and LiFePO4 end members; (b) front phase evolution during delithiation; (c) front phase evolution during lithiation. Small vertical arrows indicates the movement of (Li+, e-) pairs, the longest ones symbolizing an energetically favored extraction/insertion from/into the channels. The large red arrows indicate the direction in which the interfacial region is moving." [18]

2.2 Methods of Battery Material Study

2.2.1 Experimental difficulties

From section 2.1.2 it may be seen that the very fundamental scheme of the ionic conductivity in lithium batteries requires further work to be established with certainty. However, measurements which achieve definitive results present many challenges.

One challenge is the ability of operating a given microscopy technique in situ. Practically, when studying the charging dynamics in a battery it is most desirable to see these effects as they are occurring. Due to capacity loss and kinetics issues that are also the subject of study, when a battery is charged lithium molecules do not necessarily remain situated

in one place indefinitely. Therefore studies which charge battery materials, remove them from the charging apparatus, then examine said materials using their microscopy of choice risk viewing a sample that is not indicative of an actual step of the charging process. Also, due to questions of the steps of the actual process of ionic transport of lithium it is crucial to see the development of the charged battery step from fully delithiated to fully lithiated and the reverse at small charge increments. To achieve this, an in situ system is required to study battery materials. This requires a fully integrated electrochemical cell, and must deal with the individual constraints of the observing system.

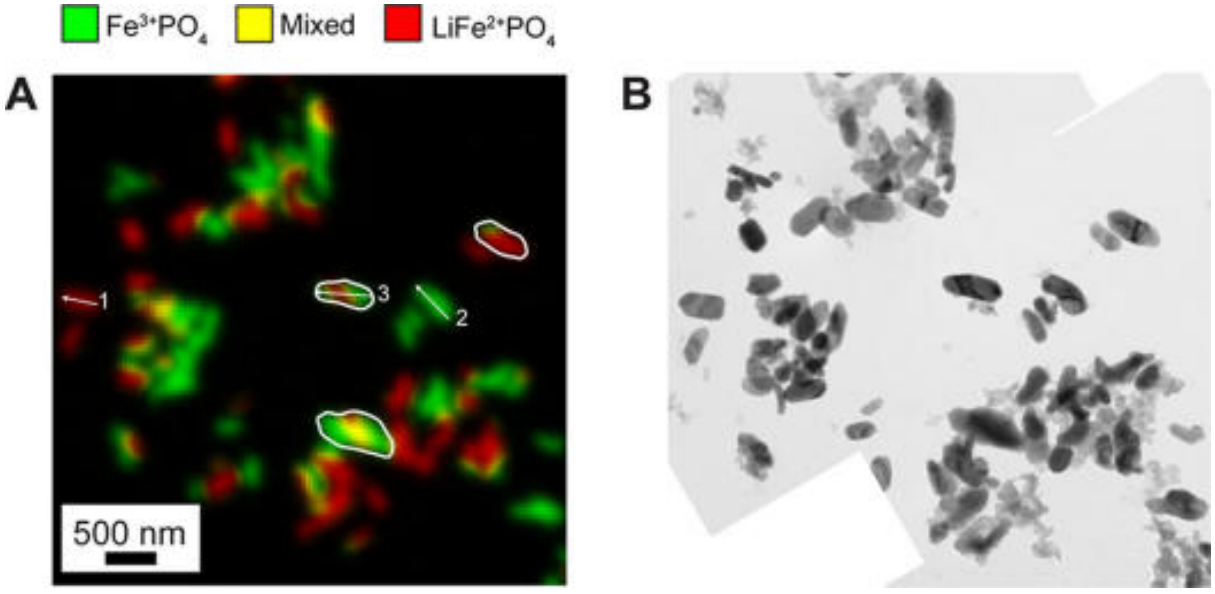

FIGURE 2.4: "(A)State-of-charge mapping and (B) morphology of lithium iron phosphate electrode powder dispersed by sonication. Outlined in white are particles in which two phases coexist within the same particle." The image was taken using oxidation-state-sensitive X-ray microscopy [19]

Another issue is the size of the sampling area. While it is important to gain experimental knowledge via in situ means, the techniques used must have comparable resolution and sample sizes to compare with ex situ measurements. While in situ oxidation state-sensitive X-ray microscopy may be performed to take clear images of the charging states of nanoparticles as seen in figure 2.4, the length scale of these measurements have a resolution of approximately 40nm [19]. At this resolution the charge state of particles may be depicted, but the atomic features are missing. This study has been used to disprove the domino-cascade model by demonstrating that charging times are not negligible in comparison to nucleation time scales, as supported by the fact that approximately 2% of the particles are in a mixed charge state. However, with greater resolution it is hoped that the ionic pathways and the resultant charged areas within these particles may be viewed.

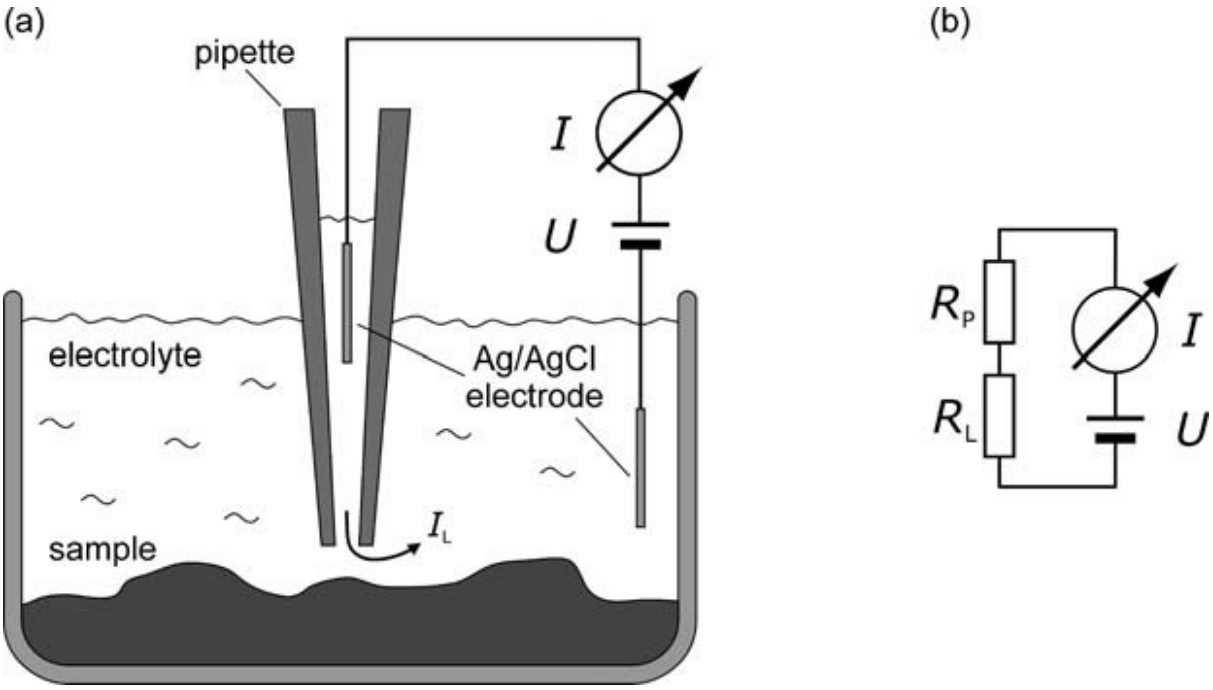

FIGURE 2.5: "(a) Schematic of a basic SICM setup for current measurements over a non-porous sample. The tip of a pulled nanopipette is brought into close proximity to the sample surface. A voltage, U, is applied between the electrode in the pipette and that in the bath, causing an ionic current to flow through the opening of the pipette tip. With decreasing tip-sample distance, this current decreases as a result of the "squeezing" of the current into a narrowing conductance path (gap) between pipette and sample. Since no mechanical contact occurs during this process until "touch-down", the measured leakage current, IL, provides a contact-free measure of tip-sample distance. By scanning the sample with respect to the pipette tip, two-dimensional images of sample topography can be recorded. (b) Equivalent circuit for this setup. The resistance of the pipette, RP, is in series with the resistance of the leakage path, RL" [21]

To perform such an experiment would also mean selectively charging the electrode material. Although in situ may refer to a battery charging scheme wherein a uniform voltage is applied across the electrode material, to see charge pathways at an atomic scale local charging is necessary to determine the path of ions in their entirety, from application to voltage bias to lithiation of specific areas of the battery materials. This is a crucial step in determining the evolution of 'hot spots,' areas which attract higher ionic charges for unknown reasons [20].

2.2.2 Scanning Ion Conductance Microscopy

2.2.2.1 Operational Principle

Scanning ion conductance microscopy (SICM) is a scanning probe method based on electrochemistry. As depicted in figure 2.5 an electrode situated inside a pipette acts as the probe [21]. A voltage bias is then applied between the electrode in the pipette and an electrode outside the pipette via the electrolytic solution they are in. Through application of this voltage, there will be an ionic current between the two electrodes. This ionic current will change as the probe changes position related to the sample surface and in accordance to the features of this surface. At a sufficient distance away from the sample surface, there will be a steady state current between the electrodes, and changes in topography during scanning will not affect this current. As the tip is brought closer to the sample if we assume the sample is an insulator, the pathway that the ionic pathway may take is beginning to be cut off by the smaller space between the nanopipette opening and the surface. This may be modeled as two resistors in series where R_P is the probe resistance, the resistance caused by the ionic path needing to pass through the small (nm) opening of the pipette, and R_L which is the leakage path resistance which is determined by the space between probe and sample that allows the ionic charge to pass. If we assume that there are some small (nm) topographic features on this insulator surface, and that the probe is scanned laterally but not vertically, then the current will change depending on the topographic height. By monitoring the current signal, a topographic image may thereby be created. However, if these features of the topography are large enough, then without any height corrections the tip will crash into the surface which may break or damage the tip or sample. Therefore, a constant height mode is often applied. In this mode, the probe is scanned over the surface while the current is monitored and maintained at a constant value. This means that the tip will always be the same distance away from the sample, and no crashing will occur.

The previous scheme assumes that the surface is an unvaried insulator with small topographic features. However, if we change this surface to a conductor with small topographic images we are able to run the same operation. One difference that occurs in the fact that instead of achieving a negative current feedback signal in terms of probe to sample distance, a positive feedback signal will be present. Furthermore, the sample surface may be a mix of conductor and insulator. If we assume that the surface is completely flat, then the positive and negative feedback mechanisms attributed to insulators and conductors means that it is possible to map out areas of insulator and conductor. If this sample has

topographic features, things become more difficult. In this circumstance a smaller distance between probe and sample may be misinterpreted as an area of higher conductivity, and vice versa. If a very high current resolution, and consequently topographic resolution is required, then approaching the surface to maintain a constant distance from a sample which is thought to be an area of lower height, but is actually an area of lower conductivity will cause a crash of the tip. That is why this technique has typically been used for biological samples where the resolution isn't as important. Biological systems studied using this method are usually quite sensitive, so the non-invasive, low energy, non-contact, micrometer resolution of this technique is more than adequate. However, for higher resolution on surface with non negligible roughness, other techniques are required for vertical height detection.

2.2.2.2 Shear Force Detection

One of the more prevalent topographic detection systems used in conjunction with SICM is shear force detection. To perform this detection a SICM set-up is used but a piezoelectric stack is attached to the base of the pipette probe. The probe which is situated perpendicularly to the sample will vibrate in a motion parallel to the sample. This motion is highly dependent on the tip sample separation. As shown in figure 2.7 the magnitude of this distance will determine the magnitude and direction of force applied at the tip [22]. This system will act as a system of coupled oscillators, one oscillator being the transverse oscillation spring constant and the other being the force between tip and sample. By oscillating the tip at its resonant frequency and monitoring the change in oscillation amplitude as the tip enters the non-contact force regime, the force may be determined. Using a set-up like the one shown in figure 2.5 a laser is shone on the pipette tip, and the resultant diffraction pattern will appear on the photodiode. The position of this diffraction pattern is recorded and analyzed via a lock-in amplifier to recover the oscillation frequency and amplitude. Through this method, SICM microscopy may have a method of topography mapping which does not rely on current measurements.

This method is easily integrated into the SICM set-up and has been used to map flat surfaces with low resolution. However, this force sensing mechanism is fundamentally flawed in comparison to non-contact tapping mode of atomic force microscopy (AFM). While shear force detection incorporates oscillation in a direction parallel to the sample, AFM monitors oscillations perpendicular to the surface. Since the force gradient originates at the forces of the sample surface, the force is perpendicular to the surface. So, while AFM

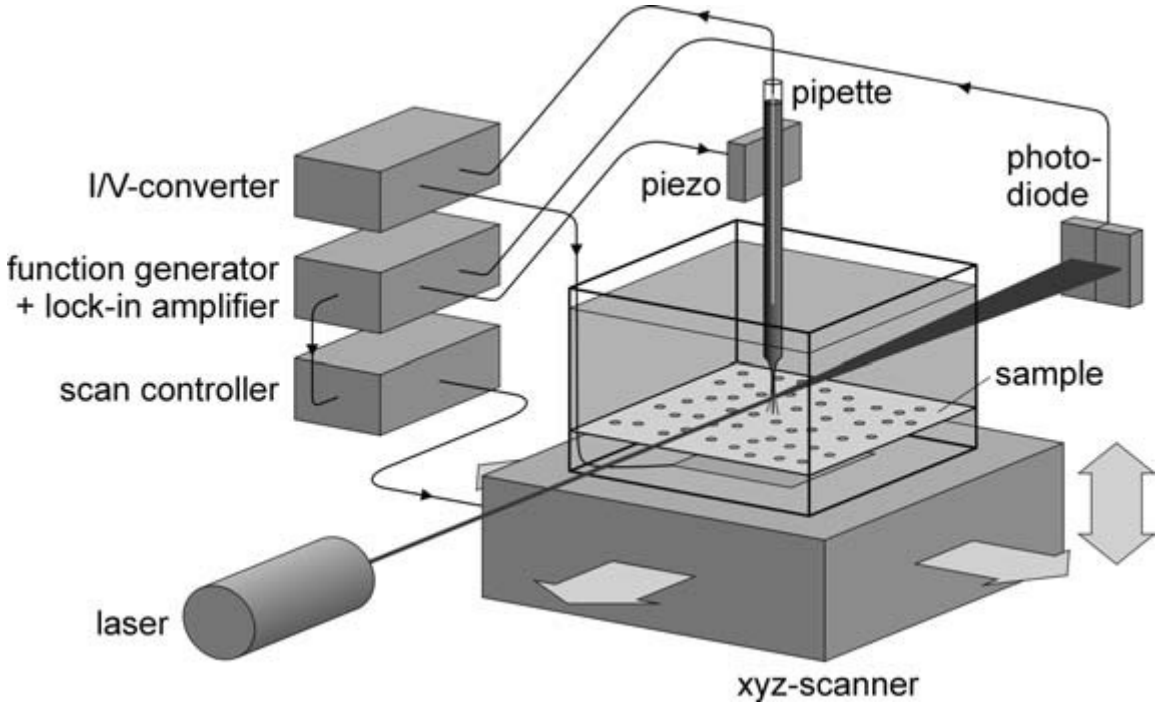

FIGURE 2.6: "Schematic illustration of the setup of a combined scanning ion conductance and shear force microscope. The lateral oscillatory motion of the probe's tapered end is induced by a piezo element to which the micropipette is attached. By focusing a laser beam on the tapered probe and detecting the diffracted light with a segmented photodiode the mechanical oscillation is converted into an electrical signal. This is analyzed by means of a lock-in amplifier whose reference channel is synchronized with the driving signal of the dither piezo. The amplitude of the probe's oscillation serves as the input signal of a feedback loop. The latter controls the vertical position of the scanner in such a way that a constant, predefined oscillation amplitude is maintained during xy-scanning. As a consequence the SICM probe follows precisely the sample topography. Simultaneously the local ion current flowing between the electrodes in the micropipette and under the porous sample is recorded. Thus possible variations in the local ion conductivity can be analyzed along with the surface topography" [21]

oscillates in this direction and travels through a certain distance of this force gradient, shear force relies on the much smaller change in perpendicular height relative to the sample that happens through the arc which the vibrating tip follows. In this way AFM is much more sensitive to topographic changes. Furthermore, due to this arc trajectory, if there is a steep feature in the topography, shear force detection will often lead to crashes of the tip. Since the tip follows an arc, and the tip will spend very little time at the furthest points of this arc from its unperturbed position. So, the interaction felt at these spots will not affect the oscillation amplitude greatly. If a feature suddenly appears it will then not affect the sensing mechanism to a large enough degree for the system to retract to a safe height, and a crash will occur as the tip is scanned parallel to the surface. This effect can be stopped by simply performing a force distance curve for every point, but

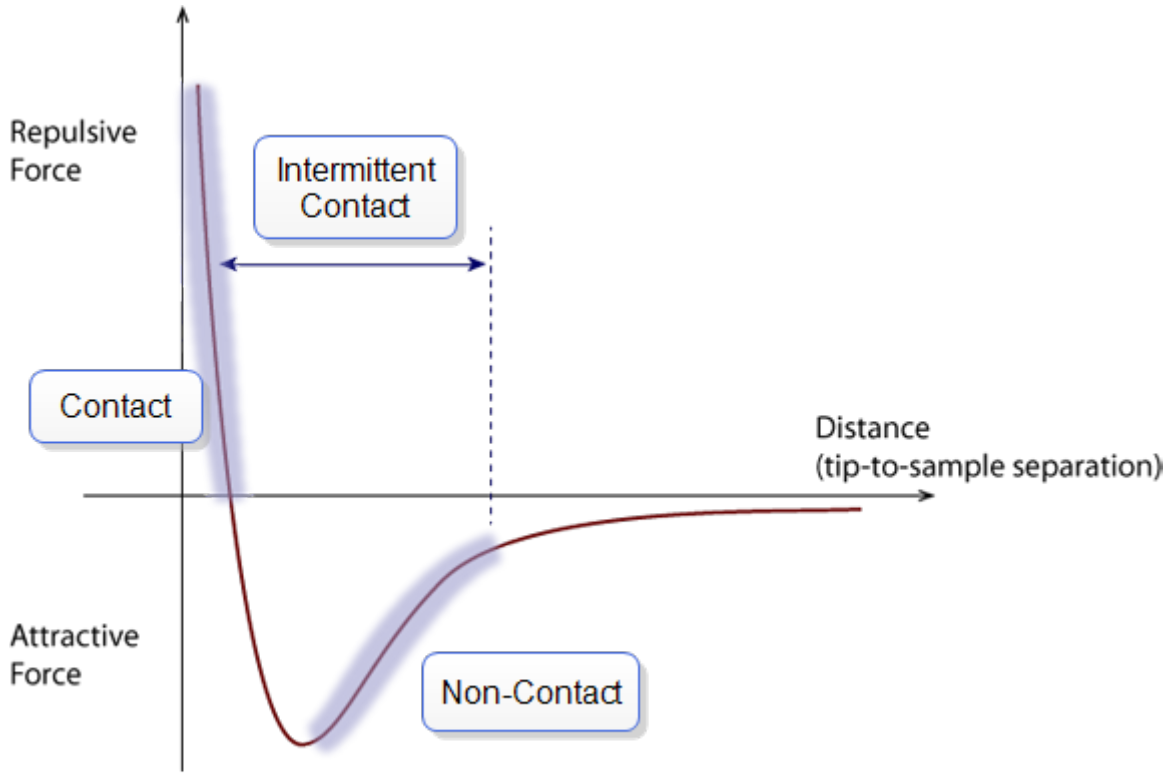

FIGURE 2.7: "The effect of tip-to-sample distance on the force interaction between tip and sample" [22]

this will increase the time per point greatly. When studying samples which change over time, this time scale may be too large to obtain valuable data.

In conclusion, shear force detection will not complete an optimal (i.e. high spatial and time resolution) topographic scan.

2.2.3 AFM

2.2.3.1 Operational Principle

Atomic force microscopy (AFM) operates similarly to shear force microscopy. The set-up, shown in figure 2.8 [23] uses a silicon cantilever rather than the pipette probe of shear force detection SICM. Here the AFM cantilever is oscillated in a perpendicular direction relative to the sample. A silicon tip pointed towards the sample will interact with said sample. To obtain the highest resolution, force must be detected over the smallest area possible. The point of the tip will interact with the sample dependent on the distance

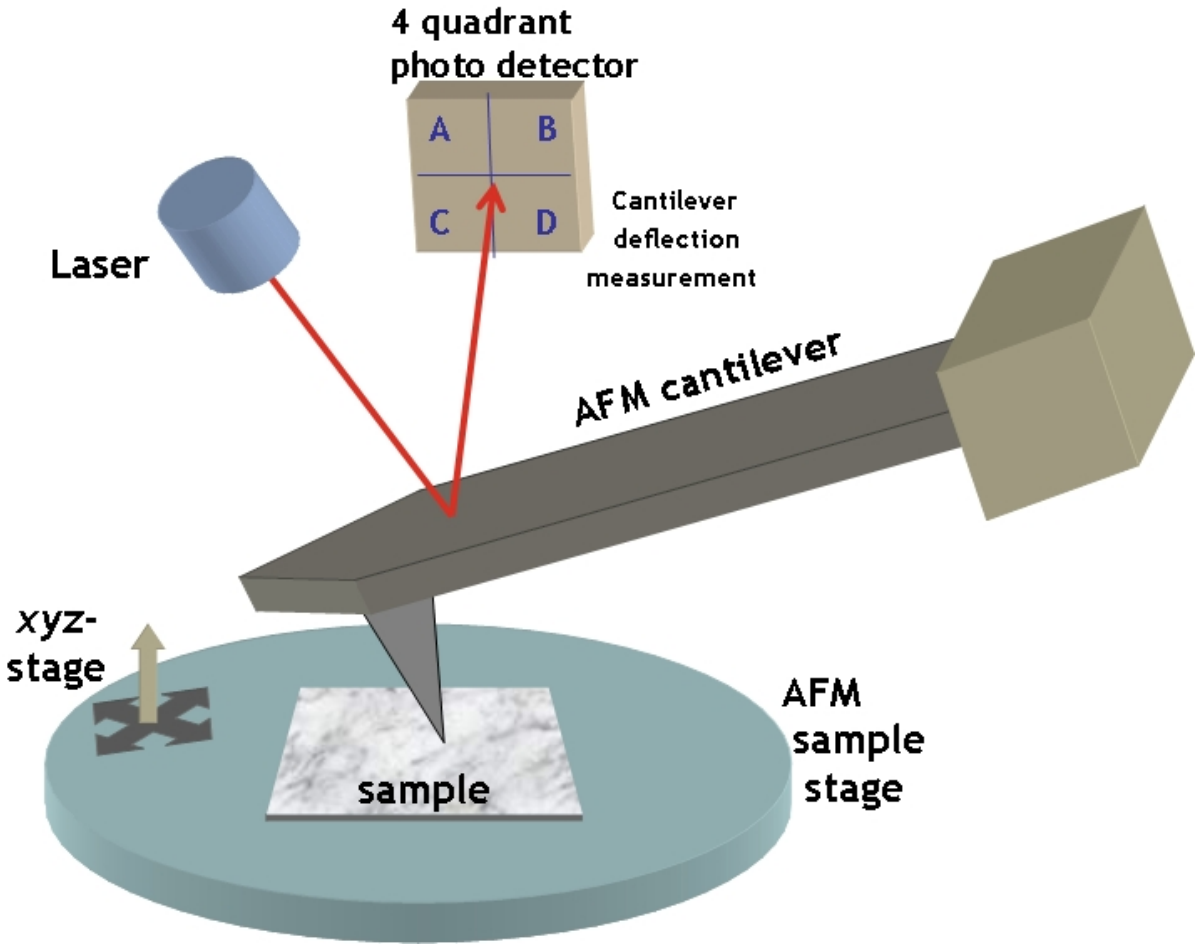

FIGURE 2.8: A typical AFM setup. The atoms at the tip of the cantilever interact with this sample. The resultant force is measured as a change in position of the cantilever. The position is measured by reflecting a laser off of the AFM cantilever, and measuring the change in position of the reflected beam on the photodiode by analyzing the four signals of the photodiode: A+B-(C+D) [23]

between the two as shown in figure 2.7. So, if a tip of the cantilever is terminated at a uniform height above the sample, but is thicker there will be more interaction between the tip and sample. This will cause an averaging of the forces exerted by the sample within this larger tip. So, resolution is determined by the sharpness of the tip and should be on the order of the size of the tip.

To sense changes in amplitude and oscillation frequency a laser is reflected off the cantilever. The reflection will fall on a segmented photodiode (this involves an optics apparatus to guide the incoming light to the cantilever, and the reflection from the laser to the photodiode as shown in Appendix A [24]). The photodiode is often split into four quadrants as shown in figure 2.8, where the electronics will subtract the sum of the top two quadrants from the sum of the bottom two quadrants $((A+B)-(C+D))$ to obtain

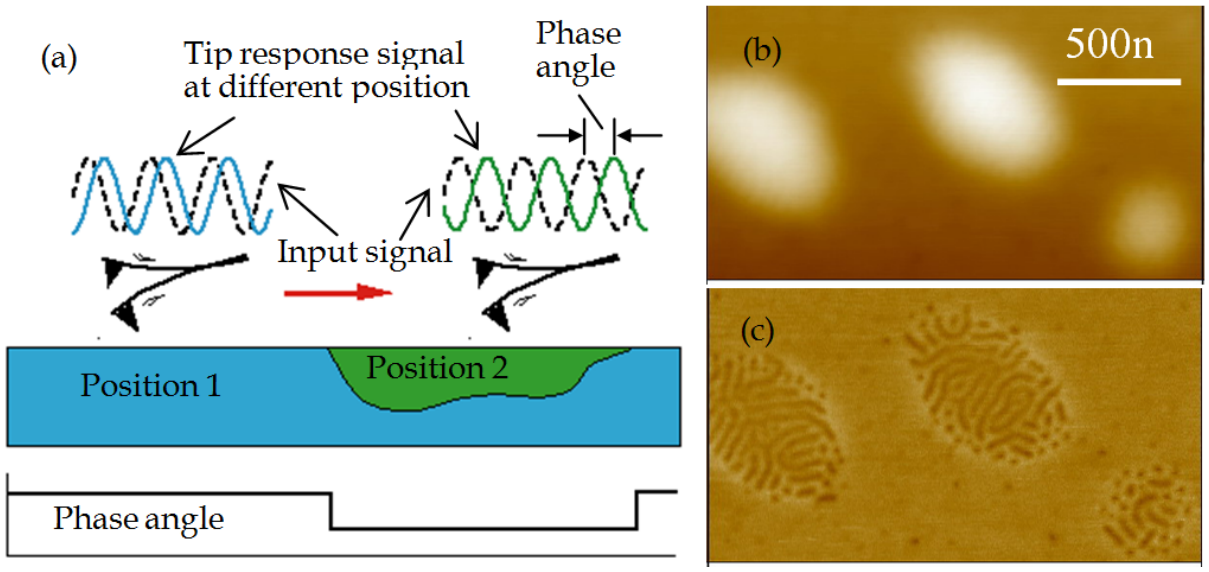

FIGURE 2.9: "a) Phase angle in TM-AFM (b) topography and (c) phase images of copolymer. The height scale is 10nm and the phase angle scale is 20°" Note that the '500n' scalebar should be read as '500nm'. [28]

a sum signal which is a representation of the deflection in a direction perpendicular to the sample. Through analysis of this signal with a lock-in amplifier the frequency components and their respective amplitudes may be measured. By observing the changes in this signal different modes of data collection have been developed .

2.2.3.2 Measurement Modes in Liquid

In the following different AFM modes typically used in solution will be described briefly. Contact does not require an oscillation of the cantilever. Instead the cantilever is brought to the surface, into the repulsive contact regime as shown in figure 2.7. Here, the signal at the photodiode will be a steady signal of fixed voltage, a direct current signal (D.C. signal). As the tip is scanned across the surface the tip will encounter topography which will apply force on the tip and cause the cantilever to bend. This will produce a change in the magnitude of the D.C. signal. Usually, the height of the cantilever is adjusted to maintain a steady current, but the amount of height the cantilever must be adjusted will be read as a change in height of the sample. Using this mode topography may be determined, however it can lead to damage of the tip or surface via the contact of the tip and surface. Also, since the tip is dragged across the surface, not only does topography affect the deflection, frictional and adhesion forces will have a substantial effect. Due to these forces absolute measurements of topographic height may be compromised.

To avoid damage of the sample or tip non-contact mode was developed for AFM. Here, the tip is oscillated at a small amplitude 50-150 Angstrom over the sample surface [25]. At this height the attractive Van der Waals forces will be detected at the cantilever as a change in amplitude due to the resonance frequency change. Yet, these Van der Waals forces are weak, leading to a small interaction force with the tip, meaning that the resolution of this method may be substantially worse than contact mode. Also, the range of the Van der Waals force gradient is on the order of 1nm, so a layer of liquid greater than this distance may dampen the small amplitude oscillations. If this occurs then the topographic image will fail to resolve the image accurately.

Tapping mode, sometimes called intermittent contact mode, involves an oscillation of the tip as in non-contact mode. In this case the amplitude of oscillation is substantially greater, sometimes up to 20nm [25], and the average height of the tip over the sample is greater. As the tip is excited to its resonance frequency it is scanned over the sample. During the scan the tip will make intermittent contact with the sample resulting in a repulsive force. This force will then affect the resonance frequency and thus the amplitude of oscillation. A lock-in amplifier is used to analyze the amplitude of oscillation, and the controller will adjust the height of cantilever to maintain a constant amplitude of oscillation. This mode allows for high spatial resolution interaction with the stronger repulsive forces while avoiding the issues of adhesion and frictional forces which affect cantilevers in contact mode.

Phase imaging is a technique which may be used in conjunction with tapping mode. The controller which sends the excitatory sinusoidal signal and receives the reflected signal from the cantilever is capable of comparing the two signals. Since the cantilever is excited sinusoidally, the cantilevers motion with force applied by the sample should be closely approximated as a sinusoid. By comparing the two signals and their respective extrema the phase difference between the two signals may be determined. This phase difference may then be used to image the sample surface. Phase data indicates the presence of dissipation forces, which may be attributed to viscoelasticity, adhesion, friction, and topometric changes such as slope [26]. Although many forces contribute to the phase image, valuable information may be extracted from the data such as that seen in figure 2.9 [27]. In this image the two phases of a co-polymer can not be distinguished via the tapping mode AFM, but the phase signal clearly defines the position of the two phases. In this manner phase imaging can be used as a method of differentiating the constituents of features with identical topography, whether it be different materials or different crystallographic orientations.

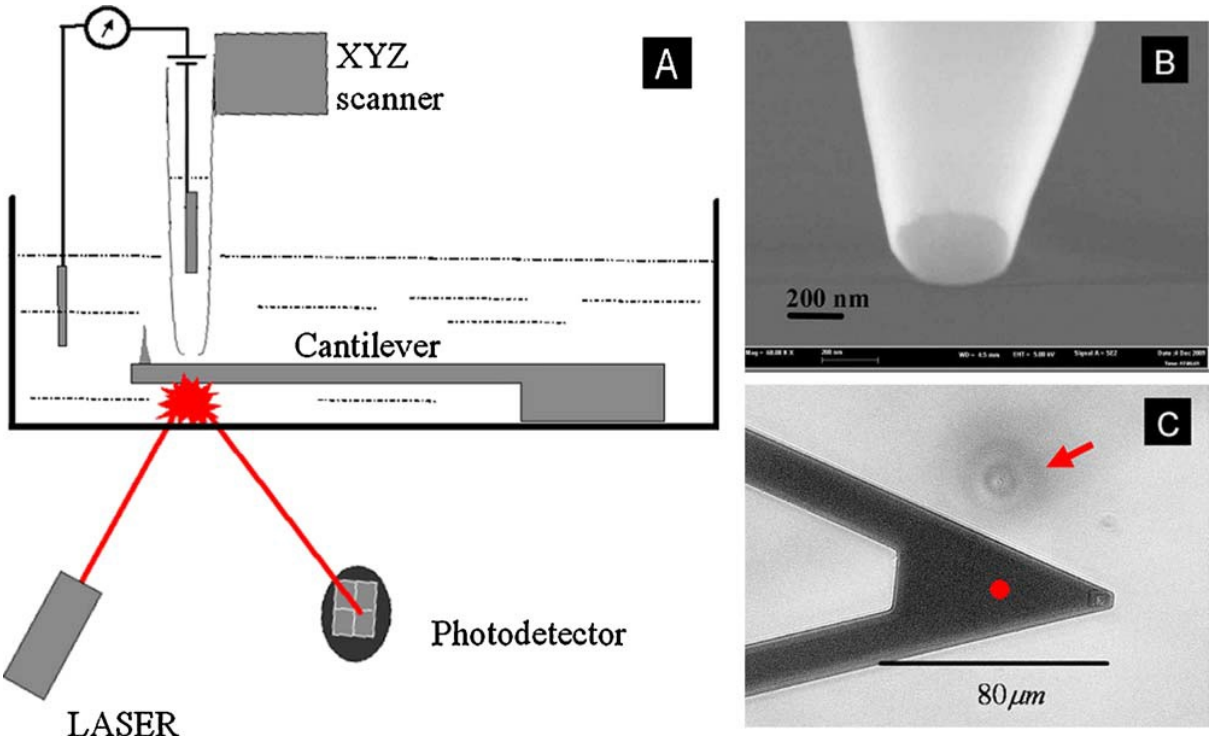

FIGURE 2.10: "(A) Scheme of our SICM–AFM setup. (B) Image of a pipette tip obtained by means of scanning electron microscopy. (C) View of a triangular cantilever and a SICM pipette (arrow) obtained by means of an inverted microscope. For imaging purposes, the pipette has been displaced in the horizontal plane from the actual position maintained during the measurements (indicated by the grey dot)."[31]

2.2.4 Combined SICM-AFM

As stated in section 2.2.2.2, shear force detection to control aperture-sample distance in SICM has some major issues. However, the intention makes sense: if a topographic measurements can be incorporated into the current sensing technique of SICM then measurements of conductivity and height will be much more reliable. A solution to the topography sensing issues of SICM has been to change the system so that AFM techniques may be used. Various mechanisms have been proposed and carried out to accomplishing this.

One method is to simply have a system where the SICM and AFM probes and sensing systems (referred to as the head) may be interchanged [28]. This allows for both measurements on the same region so both scans can be compared on one region. This system is capable of taking accurate images of identical 80 micrometer regions, with lateral resolution on the order of microns. In this situation piezo-electric drift will not have a large effect. However, if a higher resolution image on a smaller scale is performed then

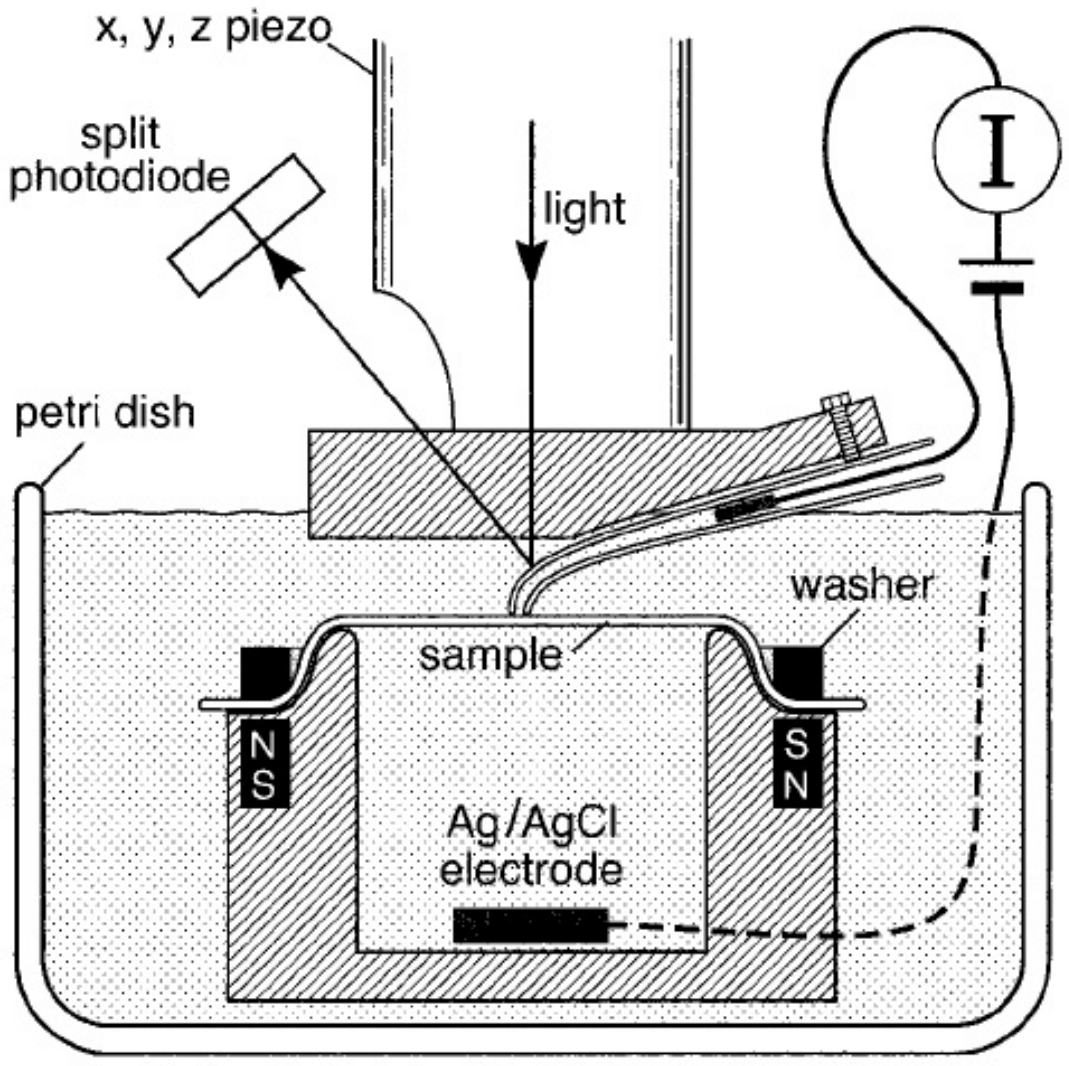

FIGURE 2.11: "Combined scanning ion conductance microscope (SICM) and atomic force microscope (AFM). A pipet is scanned over the surface of the sample and the conductance through the sample is recorded. The deflection of the pipet, measured by a light beam reflected from the pipet, is held constant by a feedback loop."[32]

drift will mean that the tip holder on the second scan will be displaced a non-negligible amount. Depending on the drift on this system this could lead to entirely different scan area. Also, the mechanism of switching tips will need to employ new techniques in order to ensure that change in probe from AFM cantilever to SICM pipette does not lead to a large displacement. If the sample is actively changing through these experiments then having to switch between the two tips will mean a loss of time resolved data compared to a system which could continuously take data using both scanning methods. Also, the SICM method must still make use of shear force methods since the the topography may have drifted or changed between scans so a prior AFM scan cannot be taken as completely

accurate.

Another method, pictured in figure 2.10 relies on performing SICM measurements on a cantilever sample stage [29]. The SICM probe is stationary in this configuration. The sample, which is mounted on a cantilever moves in reference to the SICM probe. The cantilever may be moved in the same way as a normal AFM cantilevers; it can be scanned parallel to the SICM probe tip opening, and oscillated perpendicularly to the SICM probe tip opening. By doing this SICM measurements may take place concurrently topography scans of the AFM sample stage. The issue with this system lies mainly in the vibration of the sample stage. To fit a sample on the cantilever then the sample must be of the same size of the cantilever. Typically, this is on the order of $10\mu m$, which means that sample placement will require microfabrication techniques simply for mounting. Though scan areas of AFM of higher resolution systems can be as small as a few squared micrometers, the sample stages are still about a centimeter squared in area. Even if the totality of the sample will not be measured, it can be mounted in the system easily without affecting image quality. If sample preparation techniques could not make and mount samples of this size, larger cantilevers would be required. Stiffness will increase as the cantilevers get larger, so the cantilever must become longer to reduce stiffness. Such a cantilever will have a lower frequency, which will slow down scanning.

An AFM setup which uses a bent SICM probe as depicted in figure 2.11 will allow all of the normal AFM operational modes described above to be used [30]. The only difference is that SICM functionality may be used concurrently. The pictured set-up has two potential issues: piezo-electric excitation and the long pipette cantilever. In a liquid electrochemical cell, all electronics must be sealed off completely to avoid electronic shorts which will cause damage to the system which may seriously impair its functionality. This is challenging to achieve with a piezo-drive system, such as an AFM with coarse sample approach mechanism, exchangeable AFM cantilever, and scanned samples, watertight sealing is difficult to accomplish. The pipette, as it is shown in figure 2.11 is quite long in comparison to a typical AFM cantilever. This means issues with stiffness, oscillation frequency, noise sensitivity, and spatial resolution.

2.2.4.1 Advantages of the Proposed SICM-AFM Microscope

Shown in figure 2.12 are images taken via a sequence of images of SICM, AFM, and SICM [28]. By employing both measurements key information can be derived. Here, AFM scans show much thinner fibroblasts than SICM scans. By repeating the measurements

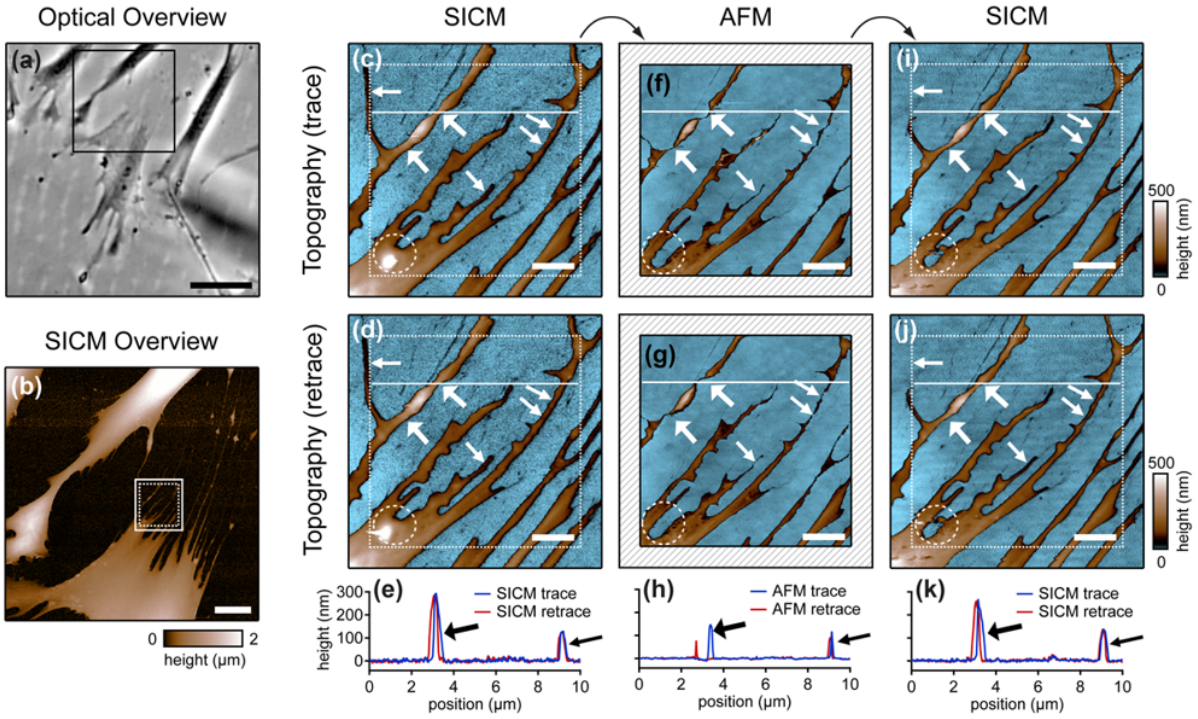

FIGURE 2.12: "Imaging of small cellular extensions. (a) Optical phase contrast overview image of fixed fibroblast cells. (b) SICM overview image of the boxed region in (a). The following SICM-AFM-SICM image sequence was acquired in the boxed region, where the SICM scan area (solid box) was slightly larger than the AFM scan area (dotted box). (c, d) Fibroblast extensions were imaged by using SICM first. Both the (c) "trace" image (where the probe moved from left to right) and the simultaneously recorded (d) "retrace" image (where the probe moved from right to left) are shown. (e) Respective height profiles along the horizontal lines in (c) and (d). (f, g) In the subsequent AFM images the features appear significantly lower and narrower (diagonal arrows). Weakly attached sections are shifted laterally by the AFM tip (thick arrows). These observations are also apparent in the respective height profiles (h). (i, j) SICM images and (k) height profiles recorded after the AFM images. The weakly attached sections appear stable again (thick arrows). However, one extension (horizontal thin arrow) is missing, suggesting that it was removed during AFM imaging. Furthermore, another extension (dashed circle) might have been permanently damaged by AFM imaging. Scale bars: $40\mu m(a), 10\mu m(b), and\, 2\mu m$ (c, d, f, g, i, j)." [29]

it was seen that after an AFM contact mode scan the SICM scan sees the fibroblasts as thicker than that shown in the AFM measurement, but not as thick as in the initial SICM measurement. This leads to two conclusions. The first is that the SICM sees the fibroblasts as larger features due to their ionic characteristics because the pre and post AFM scans show smaller fibroblasts. Second is that the AFM measurements harm the fibroblasts. Successive SICM scans show little difference in the form of the fibroblasts, but after the AFM scan they have changed considerably. These successive measurements give a lot of information about the system, although the necessary change of tips between

measurements introduces systematic errors that put the results of this study in question. By doing concurrent SICM and AFM on our lithium-ion battery materials we hope to see the changes that the SICM measurements make on the topographic information. Crystallographic shifts will occur when the sample is lithiated, which should be seen through measurement of topography. To see such differences both techniques are required. By incorporating the two together into one system things may happen faster, and with less disturbances to the sample in comparison to the system which requires switching from SICM pipette to AFM cantilever.

The microscope being developed in this study is most similar to the combined AFM-SICM microscope shown in 2.11. The designs for the system are shown in Appendix A. There are a few key differences between the previously described systems and this one, the main ones being electronics, photothermal excitation, and tip design. In terms of electronics, this SICM measurement system is making use of a retro-fitted electrochemical atomic force microscope designed and built by Aleks Labuda [24]. Due to the rigid design, optical system, and electronics incorporated into the sytem topography can be measured with sub-nanometer resolution. Most of the studies which have previously made use of SICM techniques achieved resolutions of the order of micrometers. Next, photo-thermal excitation is used instead of piezo-electric excitation. By modulating the intensity of an excitation laser incident on the pipette probe one side of the pipette should heat up compared to the other side. This heating will cause expansion which will bend the cantilever. As the amplitude of intensity of the laser decreases over its sinusoidal cycle the pipette will cool and return to its initial form. This will result in an oscillation of the cantilever such as is done by piezo-electric actuation. In this system the laser may be operated far outside of the range of the electrolyte the sample and cantilever are based in, pre-empting any dangers of short circuits. Also, the oscillatory excitation laser light may be placed anywhere on the cantilever via optical alignment. This leads to some powerful methods of probe creation. Instead of the large centimeter long probes used in SICM, pipette probes may be created, bent, then fixed close to their tip, and excited at an area nearest their base. By doing this, cantilever of much smaller dimensions can be used. To obtain comparable resolutions to silicon cantilevers this is a necessary step which has been lacking in previous SICM-AFM studies.

2.2.4.2 Probes

To make use of an integrated SICM-AFM system a probe must be used which fulfills both AFM and SICM scanning criteria. There are no such cantilever or SICM tips on the market which fit these criteria. These tips must be built in the lab with the following demands in mind.

The tip must be hollow so that fluid may flow through. To apply an ionic current via the tip a lithiated electrode will be placed in the pipette cantilever, and electrolytic fluid will carry the ionic current to the sample. To avoid electrochemical reactions, the tip must also not react to the electrochemical current. So, the pipette is made of glass, as are used with SICM tips. SICM tips are usually made of pulled borosilicate or quartz capillaries. Capillaries become pipettes with sharp tips when pulled under tailored conditions for the specific glass type and capillary size.

The sharp tip of pulled pipettes used in SICM is required here as well. A smaller tip is beneficial for higher resolution SICM measurements because the diameter of the tip opening determines the resistance of the pipette, and the resolution of the current measurements. For this reason tip openings of SICM tips measures 30-100nm in diameter.

AFM cantilevers also have sharp tips. The radius of these tips is typically on the order of 0-1nm. The size of this tip should be on the same order as the lateral resolution of this technique. A smaller tip is preferable for both techniques.

The geometry of SICM and AFM probes is fundamentally different. SICM probes consist of a cylinder tapered to a cone at the apex. AFM tips vary in shape, but the tip is not at the end furthest to the fixed end as it is in the SICM probe. Instead it is placed on the surface directed toward the sample surface. In this way, if a probe were to be made of pipette, the end of the pipette would need to be bent downwards to interact with the surface. Furthermore, the angle between cantilever and tip must be 110° so that the tip of the cantilever is completely perpendicular to the sample. The sample stage itself actually forms a 70° in reference to the incoming detection laser. It should be noted that the reason for the tilted sample stage concerns the geometry of silicon cantilevers. As the actual tip of the cantilever is typically around 10 micrometers in height, a parallel configuration of sample stage and cantilever would incur collisions between the sample stage and cantilever chip or chip holder if any of these constituent parts are of a height greater than 10 micrometers. To avoid these issues the tip and sample stage are not parallel to ensure that the tip is the only part of the cantilever interacting with the

sample. In the AFM used in this study the sample is tilted rather than the cantilever in reference to the detection laser. The tip itself is actually perpendicular to the sample to ensure that the smallest volume of the tip apex interacts with surface, which is necessary to attain the best resolution possible.

The resonance frequency of a cantilever has a direct effect on how quickly a surface may be scanned. Over an oscillation cycle the tip will only be affected by the surface when it is closest to the surface. So, the resonance frequency gives the rate at which the cantilever comes into contact with the surface per second. Intuitively, if the tip is scanned faster over 2 pixels of output in the time it takes the tip to leave the sample and return once, then the scan area coordinated to one of those pixels will simply not be measured. Furthermore, one approach of the cantilever to the surface may not be enough to come into equilibrium into the new topography height. So, many oscillations are required to re-establish equilibrium via the feedback controller loop. A higher resonance frequency of the cantilever thus means that a larger area can be scanned in the same amount of time. AFM cantilevers have a wide range of oscillation frequencies, kilohertz to hundreds of kilohertz.

To determine the oscillation frequency of a cantilever before production it may be calculated. Initial attempts at calculating the proposed probe as shown in A.5 were completed through COMSOL Multiphysics, a finite element analysis simulation software, by Sankha Mukherjee. As shown in figure 2.13 resonance frequencies and the shapes of the oscillation modes can be modeled to provide an indication of the viability of a probe before fabrication. This provides crucial input on the critical dimensions needed to achieve the required mechanical properties.

The frequency may also be calculated from close form formulas which don't take into account all of the geometrical features of this probe, but are able to produce good approximations of the resonance frequency. The formula for the fundamental resonance frequency is given as [31]:

$$f_n = \frac{K_n}{2\pi}\sqrt{\frac{EIg}{wl^4}} \tag{2.1}$$

Where n is the mode number, K_n is a constant coordinated to the mode number, E is the Young's modulus, I is the area moment of inertia, g is the gravitational acceleration of earth, w is the load per unit length, and l is the length of the cantilever. In this case, the cantilevers will need to be hollow cylinders. The area moment of inertia for a hollow cylinder is [32]:

$$I = \frac{\pi}{4}\left(R_O^4 - R_I^4\right) \tag{2.2}$$

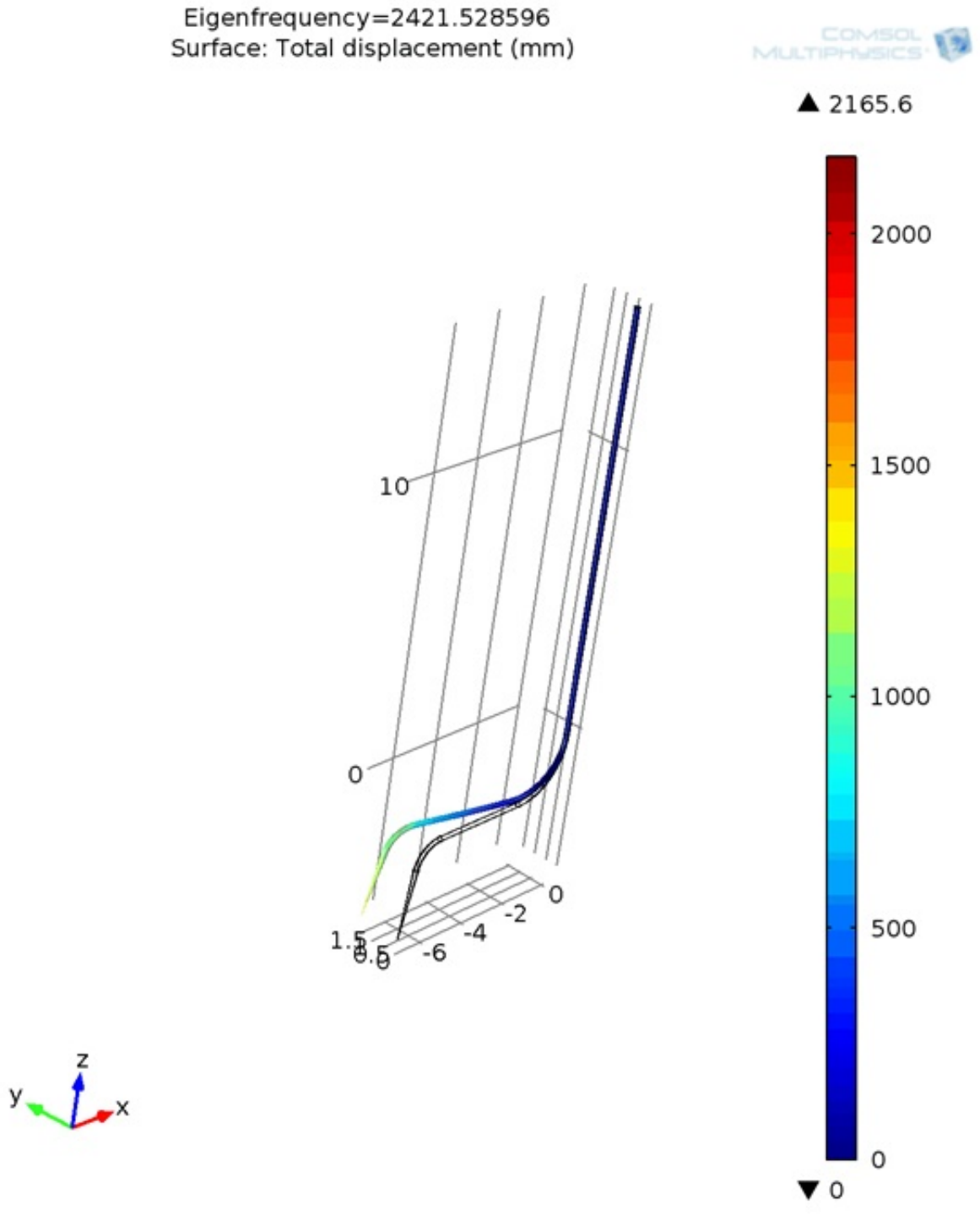

FIGURE 2.13: A COMSOL Multiphysics model of the proposed SICM-AFM probe demonstrates the displacement the tip during oscillation at the first mode. The plot accesses are given in millimeters and the colored scaled bar is given in micrometers. The modeling was done by Sankha Mukherjee.

Where R_O is the outer radius of the cylinder and R_I is the inner radius of the radius. The formula for load per unit length for an annular cross-section is [31]:

$$w = \pi \left(R_O^2 - R_I^2\right) \rho g \tag{2.3}$$

Where ρ is the density of the material. Subsituting equation 2.2 and equation 2.3 into equation 2.1 and using the K_n for n of 1, the fundamental frequency, produces the expression:

$$f_n = \frac{3.52}{2\pi} \sqrt{\frac{\left(R_O^4 - R_I^4\right) E}{\left(R_O^2 - R_I^2\right) \rho l^4}} \tag{2.4}$$

Using this we can see that to increase resonance frequency the length should be shortened, the cylinder walls should be thicker, and the outer radius should be increased. Frequency is not the only quantity which needs to be considered. Stiffness is also important; a stiffness of over 100 N/m will be too stiff to have an easily detectable deflection. When the tip-sample force gradients exceed the cantilever spring constant there will be mechanical instabilities. Typical gradients for van der Waal or electrostatic interactions are less than 0.2N/m. The formula for stiffness is [33]:

$$k = \frac{3EI}{l^3} \tag{2.5}$$

Then subsituting in the area moment of inertia for a hollow cylinder the equation is:

$$k = \frac{3\pi E \left(R_O^4 - R_I^4\right)}{64 l^3} \tag{2.6}$$

Here it can be seen that a longer cantilever, thinner cylinder walls, and a smaller outer radius will decrease stiffness. So, depending on the material properties and constraints of the processing of these cantilevers, the stiffness might need to be decreased or increased to be of an acceptable value, which cannot be accomplished while increasing resonance frequency indefinitely.

To measure this resonance frequency a laser spot is reflected off the cantilever which is made of silicon. The obtain a reflection from these cantilevers an analogous surface must be maintained on the probe surface. A non-reflective surface will be of little use, and a rounded or rough surface will disperse light so that the collection efficiency at the photodiode is too low to detect the small differences in signal at each photodiode quadrant.

All of these issues are crucial in designing and creating integrated SICM-AFM probes.

Chapter 3

Experimental Methods and Instrumentation

3.1 Materials

Suitable probes must be created in order to perform integrated SICM-AFM measurements. SICM tips are often made from pulling pipettes using a pipette puller and capillary tubes. With this mind, the following were the materials chosen to create the new probes.

3.1.1 X-Ray diffraction tubes

X-ray diffraction tubes fabricated by Charles Supper Company were purchased. Three types of tubes were purchased, those made of boron rich glass, quartz, and the company's 'Special Glass'. As seen in figure 3.1 these tubes have a larger neck diameter of 8mm, which is quickly tapered to a size on the order of millimeters. It then tapers slowly to 100 micrometers in size, and the last few centimeters of the tube are within a few micrometers of being 100μm in diameter. These were chosen due to their uniform and micrometer sized diameters.

FIGURE 3.1: An X-ray diffraction tube is shown here. The diameter of the tube is 8mm at the left side, quickly tapered to mm size, then more slowly tapered 100 μm outer diameter with 10 μm thick walls.

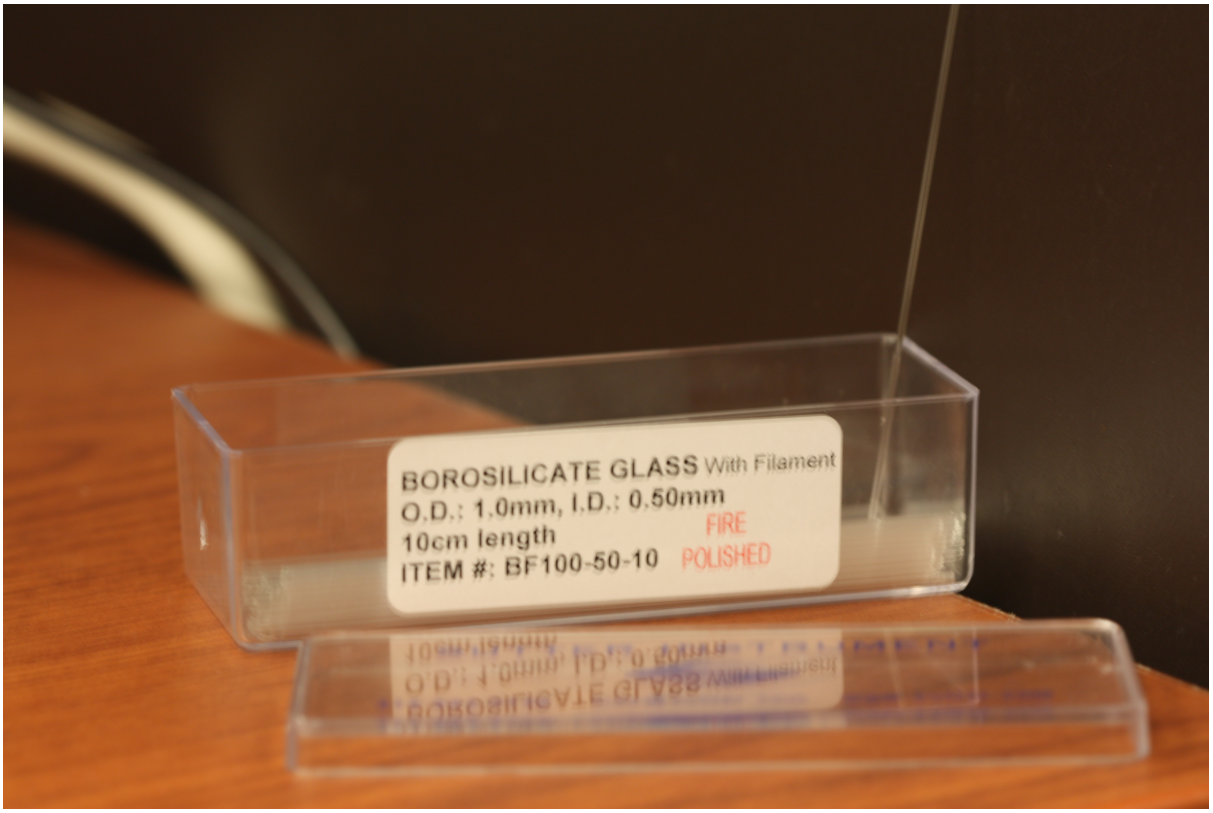

FIGURE 3.2: A borosilicate capillary tube is shown here with packaging. These capillaries are of outer diameter of 1.0 mm, inner diameter of 0.50 mm and a length of 10cm.

FIGURE 3.3: A P-87 pipette puller. The two metallic bars are brought towards the filament housing in the middle of the puller. The large round screws tighten the capillaries into place as they are pulled and heated simultaneously.

3.1.2 Capillary tubes

Capillary tubes are pulled using a pipette puller to create pipettes. According to the pipette cookbook [34], to obtain long (mm) and sharp (tips of 30-100nm) these pipettes are required. As seen in figure 3.2 the tubes are borosilicate glass with filament. The filament increases the hydrophilicity of the inner surface of the tubing, increasing the flow of liquid through the tube. The outer diameter is 1.0 mm, the inner diameter is 0.50 mm, and the length is 10 cm.

3.2 Fabrication of Probes

3.2.1 Pipette puller

To taper the capillaries into pipettes a pipette puller is created. This pipette puller heats up a metal box filament which is placed around the capillary. As the filament warms up,

the capillary glass softens. Simultaneously, a weight within the puller pulls the two bars holding the capillary away from each other. Once the glass is soft enough the capillary is pulled into pipettes of similar length and size. When the capillary separates the bars return to the retracted position as shown in figure 3.3 and the heating is turned off.

The pulling process is actually programmed through the numeric interface on the right of the puller. By varying values a recipe of many steps may be created for pulling of the capillaries. The quantities which may be modified are heat, pull, velocity, and time.

The Heat setting controls the amount of electric current which is supplied to the filament heating system. Due to small differences between filaments and pullers, a ramp test is performed to find the base point of pipette recipes. A ramp test consists of increasing the heat value in increments of 5 while a capillary is in the pulling position. When the pipettes are finally produced the heat value is recorded. This ramp value is used as the set point, with recipes advising to use a heat value of this set point plus some integer. To work reliably this ramp test must be completed for each new capillary dimension and material.

Pull controls the force applied by the metal bars which the capillaries are screwed onto.

Velocity controls the speed at which the bars are pulled apart once the glass softens and the bars begin to spread apart.

Time refers to the time between the onset of the heat, and the pull of the metal bars.

Much work has been done to create a variety of pipettes for many purposes. The Pipette Cookbook [34] collects many of those recipes in one place with detailed information on the pipettes created by using each set of steps.

3.2.2 Voltaic arc apparatus

The voltaic arc apparatus is used to melt glass, and in fulfilling this function it is used as a pipette puller and bender of the pipettes. Essentially, a highly localized electrical discharge in air between two sharp tungsten tips is used to locally heat the pipette. As shown in figure 3.4 the system consists of a stand of adjustable position in three dimensions, two electrodes held in front of this stand, a GRADRIV1 high voltage/frequency driver module, a power supply, a light source, and an optical microscope. For bending a pipette the pipette is placed on the stand using double sided tape. Using the position

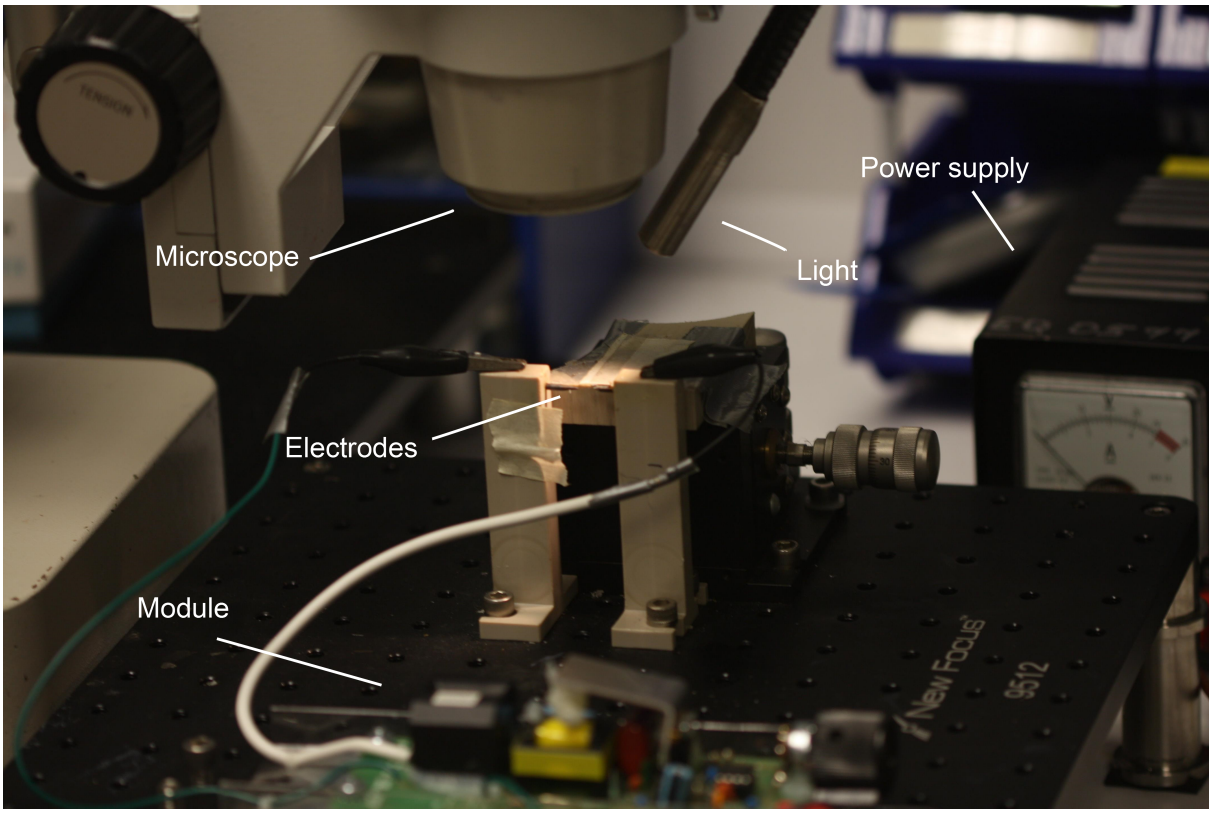

FIGURE 3.4: The voltaic apparatus consists of a set of electrodes connected to a power supply via a high voltage/frequency driver module. A microscope and light are used for viewing the bending process.

adjustment dials on the stand the position of the pipette is adjusted to the desired position. The power supply is then switched on. The current limiter on the driver module is ramped up very slowly. This is important as the current limiter will control the intensity of the power dissipated between the electrode of the voltaic arc and increasing the heat applied to the pipette tip. The heat must be controlled carefully during the bending process because while the bending of the pipette requires a certain temperature, the same heat at the nearby tip will lead to melting which may deform the tip or close the opening. Also, the heat required to melt the glass between the electrodes increases steadily as the pipettes increase in size. While the voltaic arc may be applied directly at one point on the pipette, the indirect heat at the tip nearby will be enough to melt that tip without softening the pipette at the intended bending area. One could increase the distance between tip and bending area to avoid this issue, the length from bend to tip should be minimized. Cantilever dynamics are well studied, and general motion of a generic silicon AFM cantilever can be modeled quite predictably for a given force. However, as the tip of these pipette cantilevers increase in size the model shape for the cantilever quickly deviates from the cantilever shape. As the tip becomes longer certain oscillation modes

become more prevalent, and these modes may lead to undesired or hard to predict artifacts in the topographic data obtained via these tips. So, the tip to bending area must be minimized. To do this the minimum current possible should be applied to bend the pipette. If this melts the tip then the length between bend and tip must be elongated. If not, then this length should be shortened in successive bends. Once this is optimized, a slow increase of the current is required to not overshoot the desired heating amount. The bending event does not occur instantaneously at the correct current level, it happens after a few seconds at a given spot. So, the slowest current ramping possible is optimal. Using the light and optical microscope the instance of bending must be observed closely.

The voltaic arc apparatus may also be used as a vertical pipette puller. If a weight is attached to one end of a capillary and the other end is held so that the capillary is placed between the two electrodes, then an application of the voltaic arc will perform an analogous role to the heating filament of the P-87 pipette puller. The weight will act as the pulling weight of the cantilever, where the size of the weight may be varied to change the pulling force. Though this system is crude in comparison to the pipette puller, it allows for capillaries of unusual sizes to be held securely. The P-87 pipette puller is designed for capillaries of millimeters in diameter, whereas the x-ray diffraction tubes are an order of magnitude smaller. These tubes will not be held by pipette puller screw system, and the pulling force of the puller is too great for the delicate x-ray diffraction tubes. This system is much more versatile for unusual capillary sizes.

3.2.3 Aluminum evaporator

To increase the reflection of the cantilevers and their reflectors and to increase the photothermal excitation efficiency, a thin aluminum film must be deposited on the probes. To do this batches of cantilevers and reflector material (see 3.2.5) are taped with carbon black tape or Kapton tape to a glass slide. This slide is placed in the holder, as can be seen at the top of figure 3.5. In this configuration, only the side which the AFM detection laser will be incident on (the half of the cylinder opposite the tip) will be coated. The system is pumped down to a pressure of 10^{-7} and a current is applied through the heating coil which evaporates aluminum which has been mounted on the coil. The coating is deposited at 20 nm/s to form a coating 100nm thick.

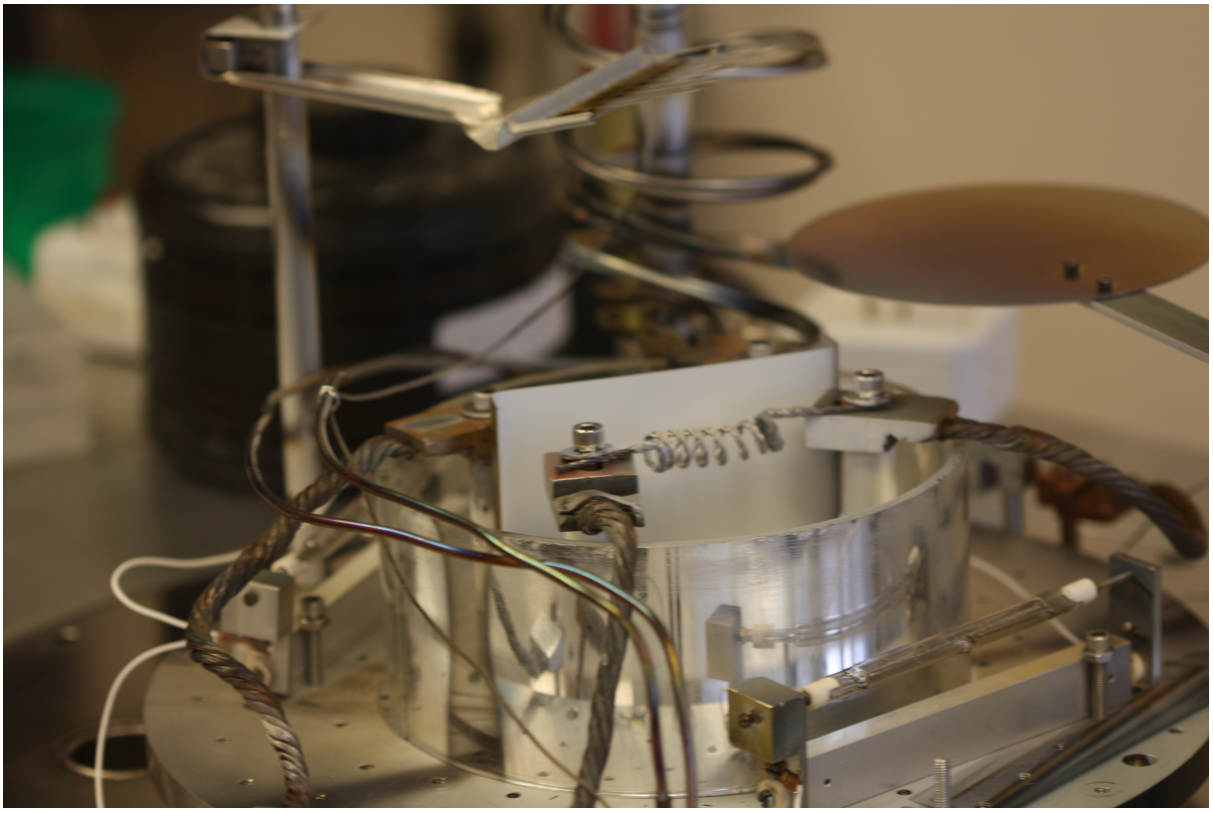

FIGURE 3.5: The aluminum evaporator includes a glass slide holder, shown at top, which holds pipettes on glass slides. directly beneath this is the heating coil where aluminum is mounted for evaporation.

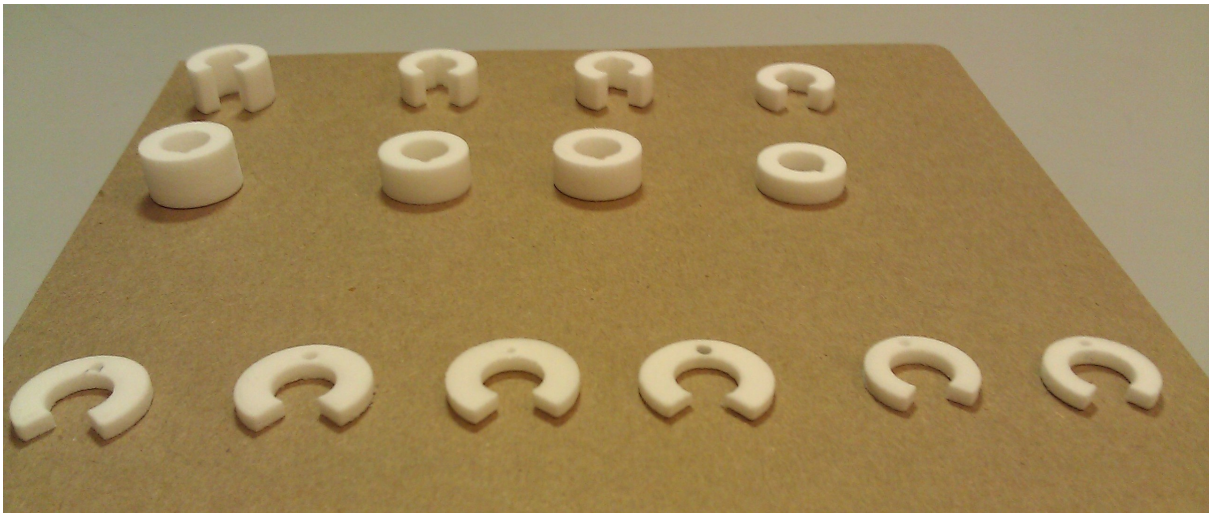

FIGURE 3.6: Printed poly-carbonate retainers of different sizes and shapes used to clamp onto the optical rod of the AFM head and hold the probes in place.

3.2.4 Mounting of probes

Two methods were used to mount the probes, chips and retainers. The first being printed retainer as shown in figure 3.6. From the design of Aleks Labuda shown in figure A.5 a retainer is required to hold the probe to the optical rod of the cantilever head. Many variations of the retainer with different inner diameters, outer diameters, and thicknesses were designed and sent to Shapeways which printed the retainers via poly-carbonate three dimensional printing. To mount probes the retainers were first placed onto the optical rod and a probe was positioned in the holder and held there by a metal clamp. LePage Professional Speed Set Epoxy was applied to fix the probe to the retainer. Once the glue was cured the metal clamp leaving a mounted probe behind.

To mount the probes to silicon chips the fibers were attached to a stage which moved in three dimensions with a certain length (5-10mm) of the pipette hanging over the edge with the tip pointing upwards. This stage was then lowered into the v-groove of a silicon chip. Three different glues were used to fix the probe in the groove.

LePage Professional Speed Set Epoxy was used for in quick 5 minute set time. However, it is quite elastic, so the probe was not rigidly held. Due to movement of the probe use of this glue was discontinued.

Epo-tek H20-E electrically conductive silver epoxy was used because of rigidity which which it holds the probe. This glue requires short cure times at high temperatures. However, if successive tips are being created the heating apparatus must be cooled again before it is reheated; if this is not done and the glue is applied to a hot surface then the glue will not adhere well to both surfaces and the two will not be held together. Also, this glue is electrochemically active, which is a large issue for the integrity of the future SICM measurements.

Norland Optical Adhesive Ultra-Violet curable glue was finally used due to its short cure time, high rigidity, and lack of electrochemical reactivity.

To mount these chips to AFM head the Speed Set Epoxy was used to glue the chip to the face of the optical rod. This glue is easily removable, so old tips may be removed from the optical rod. Such a configuration in shown in figure 4.7.

3.2.5 Reflectors

In some iterations of the fabrication process, reflectors were created to be mounted on the probes. To be useful these probes need to be highly reflective, smooth, low in mass, and be affixed perpendicularly to the incident AFM detection laser. Schott D263 T Thin glass was chosen due to its thickness of 30μm, and was coated within the aluminum evaporator to create a reflective surface. Then a section of the mounted probe was lowered onto the reflector by a stage with positional adjustment in three dimensions. By mounting both the chip and the reflector on stages, the two could be assumed to be parallel planes. Since the chip is mounted on the quartz rod of the AFM head, this mounting should ensure that the cantilever may be positioned within the cantilever so that the detection laser is bounced off the reflector co-linearly with the incident beam. This will ensure that the reflected beam will fall entirely on the photodiode and thereby produce a current signal at the photodiode of maximum amplitude.

Once positioned a glue from section 3.2.4 was applied and cured in that position.

3.2.6 Polishing Pads

One solution to the reflectivity issue was to use polishing pads to make a flat area on the pipette surface. By using a small grit to sand the pipette it was thought that a flat surface of minimal roughness could be created. Once this surface was coated with aluminum it could be used for reflection of the detection laser.

Polishing pads of 5μm, 3μm, 1μm, and 0.3μm grit size were used to polish the capillaries. Capillaries were affixed to aluminum blocks, pressure was applied as they were run over these polishing pads. The pads were used in decreasing order of grit size in order to remove a large amount of the glass, then make as smooth a surface as possible. A permanent marker was used to color the surface of the pipette. After the polishing was done the capillaries were examined under a microscope. If the marker was removed from an area it was seen as as indication that the polishing paper had removed some of the glass off the surface of the capillary.

3.3 Inspection of form

Rigorous testing and observation is required to ensure that each step of the probe creation process is successful. The following techniques were used to monitor and test the forms and physical properties of the probes.

3.3.1 Optical microscopes

A Nikon Optiphot-100 microscope with 2.5x Nikon photo eyepiece and objectives of 4x, 10x, 50x, and 100x was used to visually inspect the probes. An OMAX 5.0 USB Camera is interfaced with the microscope so that images can be taking with ToupView software. Quantitative measurements were made possible through the use of ImageJ software and a calibration sample to correlate pixels with physical units.

3.3.2 Scanning Electron Microscope

To obtain higher resolution a Hitachi S-4700 Field Emission-STEM (FE-STEM) with Oxford INCA Energy-dispersive X-ray spectroscopy was used. The microscope belongs to the Facility for Electron Microscopy Research at McGill University and was operated by Robert Gagnon who took images with direction from the authour.

Samples had to be mounted on SEM sample stages using carbon black tape as the SEM requires the samples to be in low vacuum.

3.4 Physical property testing

By using the following techniques and tools probes may be tested for their physical properties as described in section 2.2.4.2.

3.4.1 Electrochemical Atomic Force Microscope

The Electrochemical Atomic Force Microscope (ECAFM) was built in the lab by Aleks Labuda. Technical drawings can be viewed in Appendix A. Our new probes be can introduced into this system to test their physical properties.

3.4.1.1 Photothermal excitation

To test the resonance characteristics of the probe, and to use it to scan, the probe must be oscillated. The cantilever is oscillated by the Panther photothermal system as shown in figure A.3 [24]. The basic premise is that a blue laser light of sinusoidal amplitude is shone on the probe. When the laser reaches maximum intensity the probe is heated to its greatest temperature on the illuminated area and this section expands. As the laser power decreases to its minimum the area dissipates the heat quickly and contracts. This alternating expansion and retraction at a fixed frequency will cause the cantilever to oscillate at the same frequency. The amplitude of this oscillation will depend greatly on peak-to-peak amplitude of the photo-thermal power signal and the mechanical properties (i.e. Q factor) of the probe. The voltage is related to the energy of the probe oscillations. At the resonance frequency the oscillation amplitude of the cantilever may increase by orders of magnitude. A resonance peak should be observed by scanning the excitation laser through a range of frequencies in the frequency range wherein the calculated resonance frequency should occur and monitoring the amplitude response of the cantilever. This resonance frequency is then used to scan the sample in tapping mode, and the numeric value of this resonance frequency and the full width half maximum of the resonance peak yield information on the bandwidth available in scanning using the probe and the speed at which the probe may scan the surface while retaining high resolution measurements as is described in section 2.2.4.2.

3.4.1.2 Probe position detection

An optical beam deflection detection system is used to detect the deflection of the probe. While the base of the cantilever stays in the same position relative to the incoming detection laser, the probe may be deflected upwards or downwards depending on the interacting forces (photo-thermal excitation, interaction with surface, etc.). The detection beam is reflected, to a close approximation, co-linearly to the incoming detection laser. Via the polarizing beam splitter, as shown in figure A.2, the reflected laser light will be directed on the photodiode. Using the positioning screws of the AFM this reflected signal will originally be calibrated to fall on the photodiode such that the signal is maximized and centered at the middle of the four quadrants of the photodiode. As the cantilever is deflected the reflected beam will change position by a small amount so that it deviates from the original path. This will be observed as an increase in certain photodiode signals and decrease in others depending on the direction of the deflection and thus motion on

the photodector quadrants. As the probe is oscillated the sum signal (described in section 2.2.3.1) will oscillate at the same frequency with a voltage amplitude that should be proportional to the amplitude of the probe oscillation. This signal is then analyzed by the lock-in amplifier (SR-830 in this case) which performs electronic operations to apply a Fourier transform to this oscillating voltage signal. This yields the frequency components of the cantilevers oscillation and their respective amplitudes and phases. When the excitation frequency is scanned through a range of frequencies the lock-in amplifier measures the response of the cantilever at each frequency. Using this the resonance peaks of the probe may be recorded.

As the probe is scanned across the sample changes in frequency and amplitude can be used to determine tip-sample distances. By doing this the topography of the sample can be derived from the amplitude information and information concerning the dissipative forces of the sample may be recorded from the phase response.

The probes fabricated in this study must work within this framework if they are to be viable for use in integrated AFM-SICM.

3.4.2 Sample surface

DVD samples were used as tip characterization surfaces due to their well defined geometry and appropriate feature sizes.

DVDs consist of two layers of poly-carbonate material, one of which is printed with indentations called pits which are read by DVD players using a laser. The surface with pits is not exposed, so the DVD must be split apart by using a razor blade to cut through the adhesive on the circumference of the DVD. Once exposed tape is used to strip the aluminum coating of the DVD off of the surface to eliminate any non-uniformities on the surface caused by peeling of this aluminum surface. The DVD is cut to a size which may fit into the AFM, a square of $1cm^2$ in this circumstance, and is fixed to a sample stage. The DVD sample is then ready to be imaged.

The pits of the DVD vary in length, but the distance between tracks, tracks being each successive spiral of pits, is 740nm and the pits are 320nm wide and 120nm deep. With these known values scale bars of DVD scans can be made accurate, and scan dimensions can be calibrated accurately.

Chapter 4

Probe Fabrication Beginning with X-Ray Diffraction Tubes

4.1 Probe Prototype

The initial attempts at creating probes began with borosilicate capillary tubes. In these attempts the main objective was to create a hollow cantilever shaped pipette. Through experimentation with the pipette puller the capillary tubes were tapered into pipettes. Then a voltaic arc from the voltaic arc apparatus was used to bend the pipette to form a cantilever like form: a straight pipette bit with a tip extending at a 110° angle like the pipette shown in figure 4.1. An initial question was whether liquid could pass the bend to the tip of the cantilever. This is crucial as an electrode needs to be passed into the pipette with an electrolyte connecting the electrode to electrolyte outside of the pipette. If the flow of fluid were cut off then this would not be possible. Fluorescent dye was added to water which was slowly pumped into the pipette by syringe. The resultant dye marks where the liquid was able to travel. Furthermore, some of the dyed liquid could be extracted by wicking moisture at the end of the tip using a Kimwipe. This is proof that the bending of the pipette did not close the open path within the pipette.

Simply from visual inspection it is obvious to see that this bent pipette is too stiff to be a AFM cantilever. So, the next step was to find a pipette that would have an appropriate stiffness and resonance frequency for AFM tapping mode measurements.

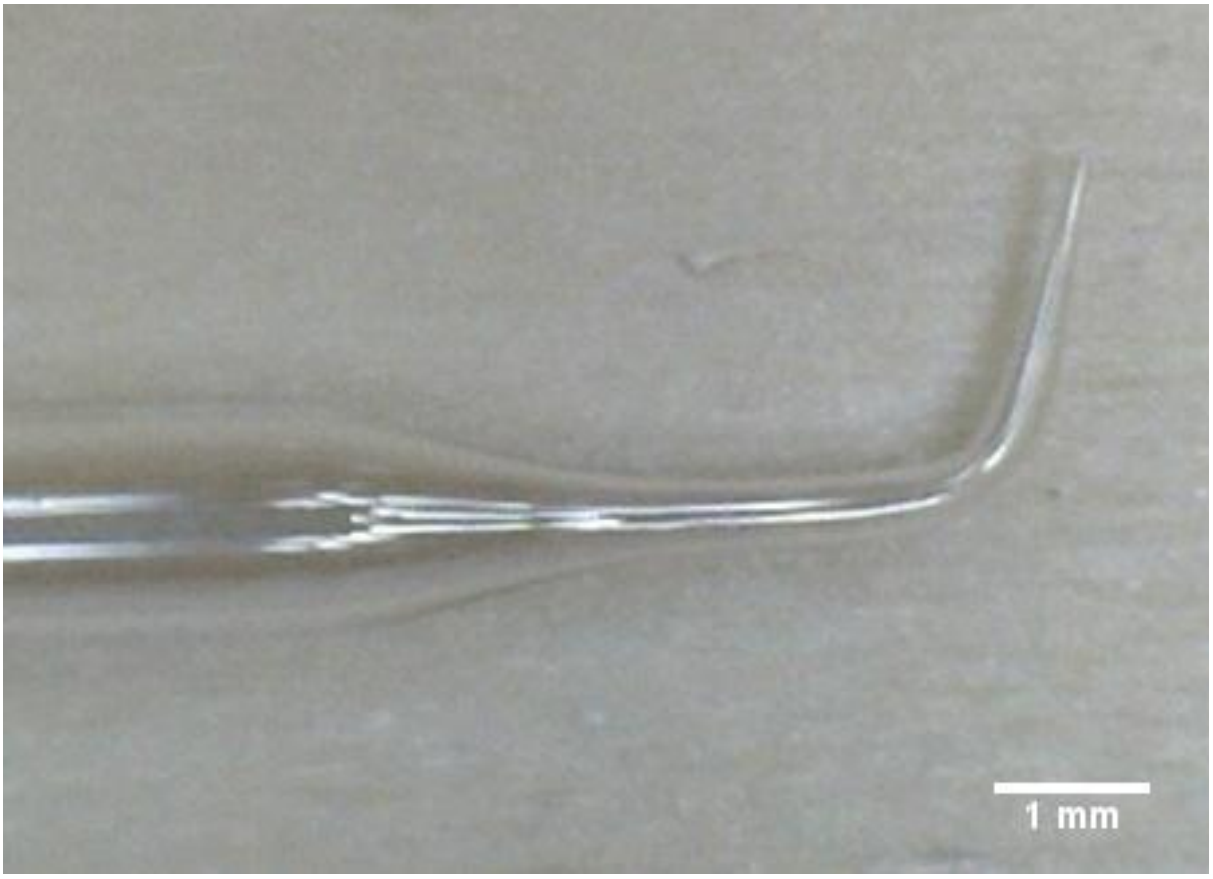

FIGURE 4.1: The first pipette probe was fabricated from a borosilicate capillary tube and was bent via the voltaic arc apparatus.

FIGURE 4.2: The first probes were filled with liquid containing fluorescent dye in order to show that liquid could pass from the large opening of the pipette, past the bend, to the tip

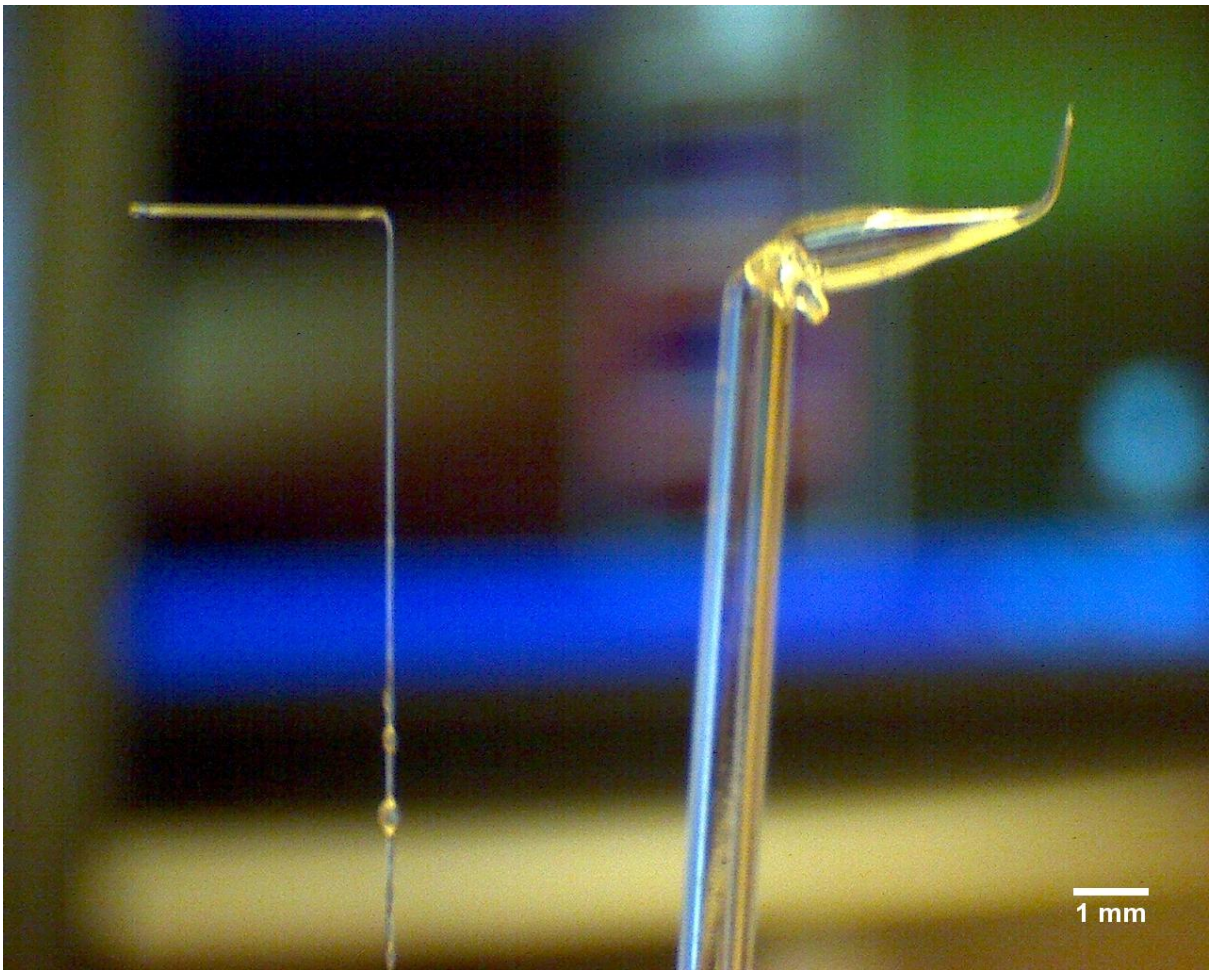

FIGURE 4.3: A side-by-side comparison of the prototype cantilever and the first tipless x-ray diffraction tube probe. Although the sharp tip had not yet been developed for the x-ray diffraction tube cantilever, this shows the size difference of the two probes and the fact that the x-ray diffraction tube may be bent without obvious deformations.

4.2 X-Ray Diffraction Tube Probes

By experimenting with the pipette puller with various recipes many shapes of pipettes were developed. However, all these tips were much too blunt to be used as a cantilever. X-ray diffraction tubes were acquired due to their small diameter. These were bent to the necessary form and a side-by-side comparison with the prototype types is shown in figure 4.3. This clearly demonstrates the immense reduction of mass between the two probes. The reduction in mass means that these tubes might fall into the range of acceptable resonance frequency and stiffness. Finite element modeling was used to test where the bends of the probe needed to be to produce an acceptable resonance frequency. The modeling, shown in figure 2.13, showed that a tip with a cantilever arm of 6mm will have a resonance frequency of 2421Hz. Probes were then created with such dimensions. Since

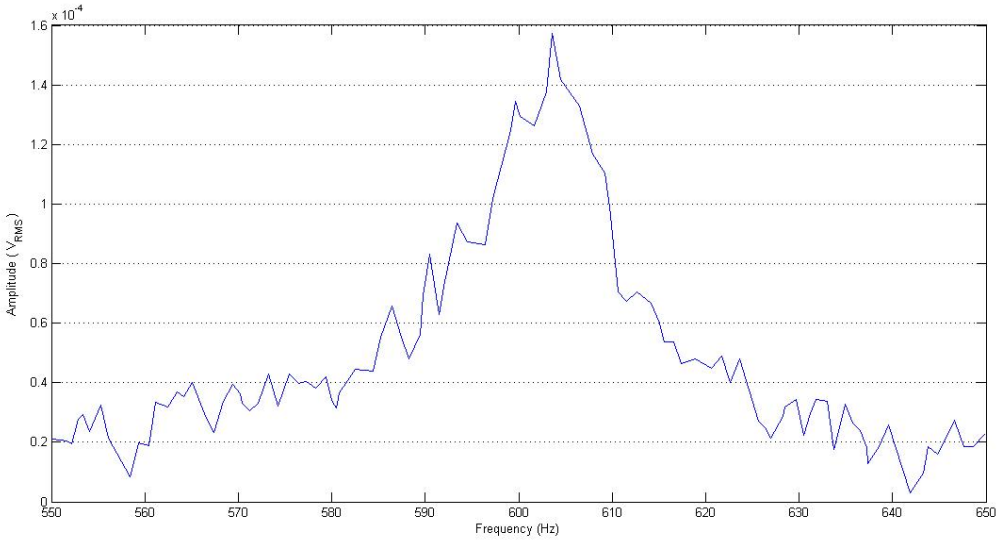

FIGURE 4.4: A frequency sweep of the first x-ray diffraction tube shown a small resonance peak at approximately 604Hz

the pipettes are transparent and the optical detection laser needs to be reflected by the probe, a reflective layer of SPI High Purity Silver Paint was placed on the probe surface through delicate application using another X-ray diffraction tube.

This probe was then mounted on the AFM head via a retainer and a frequency sweep was performed using the cantilever, yielding the data in figure 4.4. A resonance peak occurred at approximately 604Hz, although the amplitude of the signal was very low, so noise distorted the peak greatly.

A coating of aluminum was applied to the probes through evaporation as detailed in section 3.2.3. This increased the overall signal at the photodiode, and the frequency sweep in figure 4.5 shows a much larger voltage at the resonance peak in comparison to the previous cantilever. Also, the noise is much less apparent in this scan. Using this cantilever a scan was performed on a DVD sample. Several scans were performed of this DVD sample and each showed features similar to those in figure 4.6. A possible reason for these irregular features which should not appear on a clean DVD sample, as was used here, could be the effect of observing two different modes. Although the frequency sweep of this probe showed a clear resonance peak, two resonance peaks appear in close proximity. These are most likely two different mode shapes of the cantilever oscillation which happened to be close in frequency. Although the easiest system to describe and analyze would be an oscillating beam, like a silicon cantilever, the shape of these probes could lead to other vibrational modes. Instead of moving directly up and down, the long

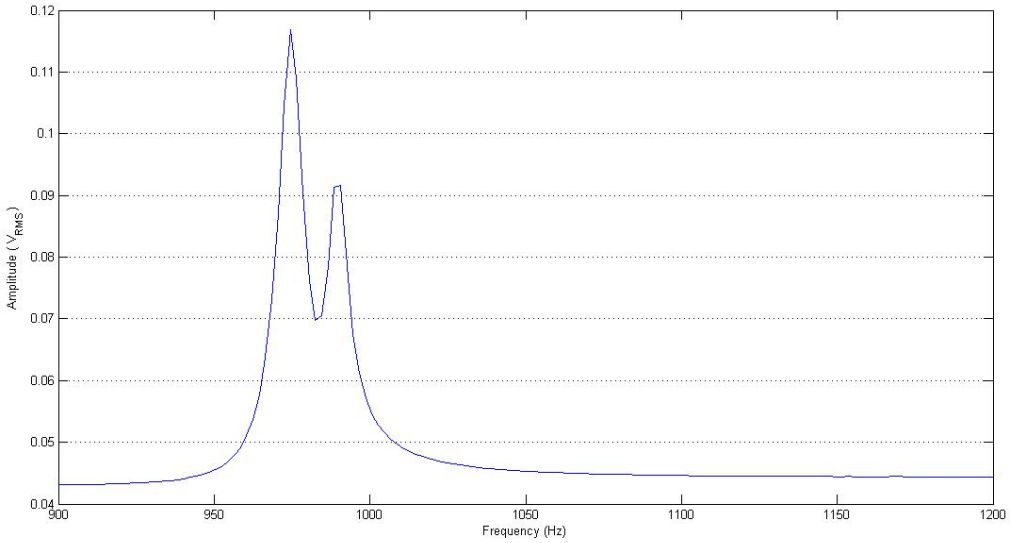

FIGURE 4.5: A frequency sweep of an aluminum coated x-ray diffraction tube probe reveals a resonance peak at approximately 970Hz with a quality factor (Q factor) of 80. The two peaks are due to slightly different vibration modes. These modes may be caused by the long tips modifying the mode shapes from that of simple beam cantilever.

tip of these probes may move horizontally, or other such ways. Then, during a scan the cantilever is maintained at a constant height by measuring the amplitude of the cantilever oscillation signal. Changes in amplitude indicate frequency shifts, which are interpreted as changes in topographic height. Here however if the the resonance frequency shifts such that the frequency crosses the minimum which appears in figure 4.5 going from right to left or left to right, then the interpretation of the topography made by the SPM controller will be the opposite of the actual changes in topography. Simply put, these two closely spaced resonance peaks must be avoided. However, they are a common occurrence in these probes. To create a cantilever with only one mode, as discussed in section 2.2.4.2, the probes must resemble typical AFM cantilevers; the bent tip of the probes must be reduced in length as much as possible. These bent tips were quite long at this point in the development process, as shown in figure 4.7, due to problems with tip melting when attempting to soften the diffraction tubes closer to the tip of the tubes.

Another possible issue could be the printed retainers. While these retainers were required to hold the probes firmly to the optical rod, the retainers design allowed for small movements due to the degradation of clamping force that the poly-carbonate structures experienced as they were adjusted to the correct position on the optical rod. Adhesives were used to mitigate this issue, but something much more solid was required. At this

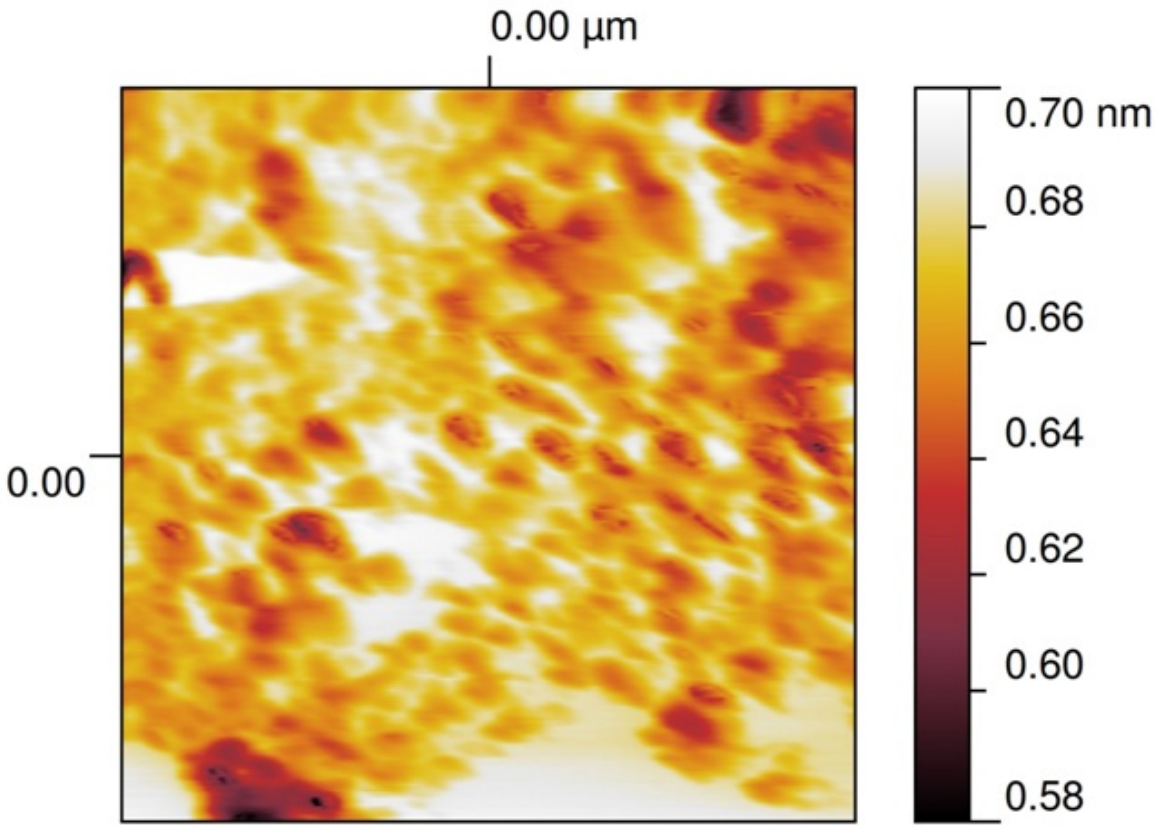

FIGURE 4.6: A topography scan of a DVD sample using an aluminum coated x-ray diffraction tube probe.

point the probes were mounted onto silicon cantilevers as shown in figure and described in section 3.2.4.

The probe mounted is this chip was also longer than previous probes. By calculating the resonance frequencies and stiffness of the x-ray diffraction tubes at several lengths using the formulas provided in section 2.2.4.2 it was determined that a probe of 5mm in length would have a resonance frequency of 4095Hz with a stiffness of 5N/m; the stiffness is within the acceptable range and the resonance frequency is higher than that of previous tips. This length was measured from where the tip was glued onto the silicon chip to the bend of the probe before the tip. The long tip was expected to have an effect on these calculations, but the calculation was simply used to direct modifications of the tip over successive iterations.

A frequency sweep was completed with this tip to produce the data in figure 4.8. The two peaks appear again, but the separation between the two has increased. The resonance

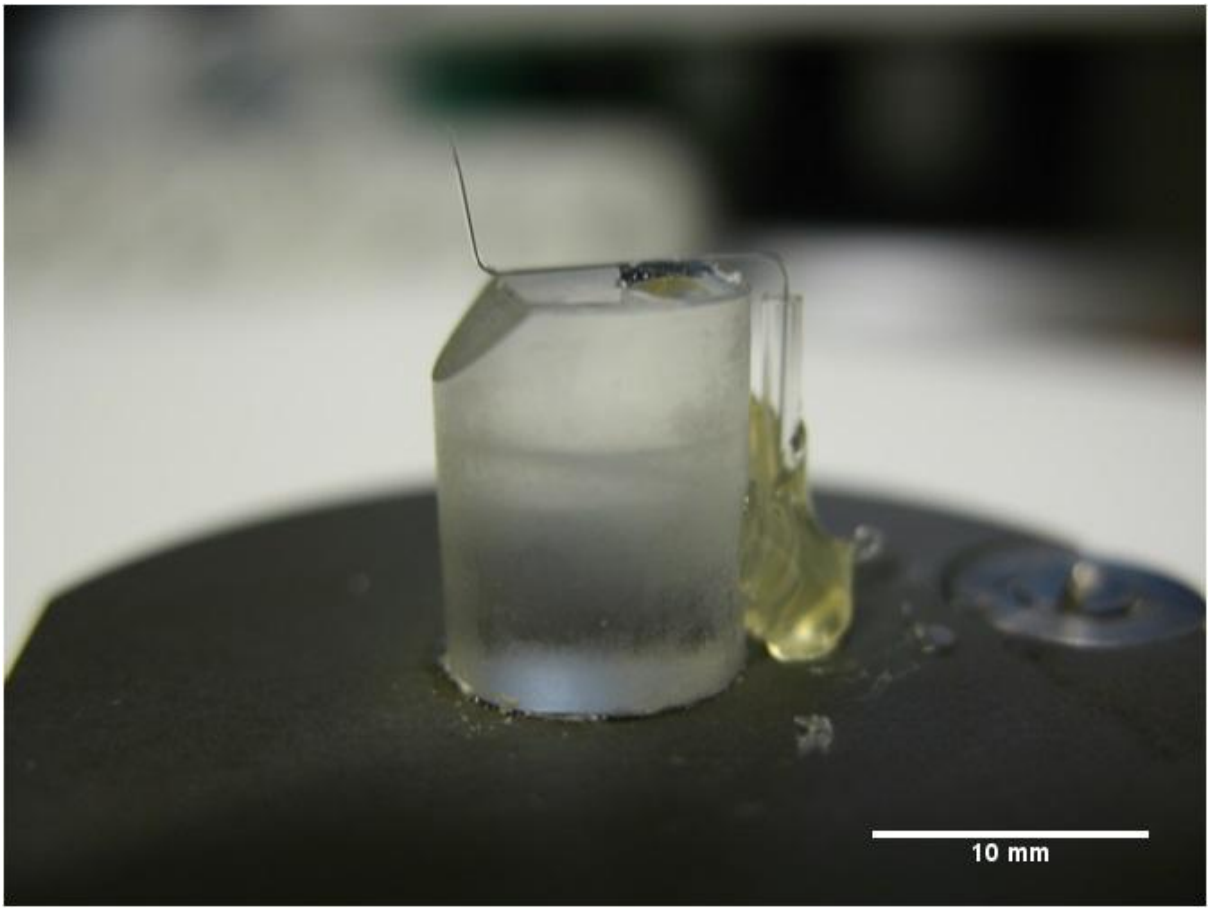

FIGURE 4.7: A x-ray diffraction tube probe mounted on a chip. The x-ray diffraction tube bends and enters a capillary (right side, with a glue base) en route to the inside of the AFM head.

frequency of the larger peak was at 4545Hz which was close to the value calculated previously.

The next issue was the low sum signal recorded at the photodiode. The reflective surface of the probe was reflecting enough of the incoming detection laser to the photodiode in order to obtain resonance frequencies via frequency sweep. However due the curvature of the tube used to create the probe the detection laser was being dispersed and the summation of the signal amplitudes of the quadrants of the photodiode were an order of magnitude less than that of a silicon cantilever in this system. A flat surface was needed for the surface. Polishing paper was used to flatten the surface of the x-ray diffraction tubes as described in section 3.2.6.

This was a difficult process due to the fragile nature of the x-ray diffraction tubes. Several of the polished tubes were used in the ECAFM, with no appreciable difference in sum signal over the non-polished probes.

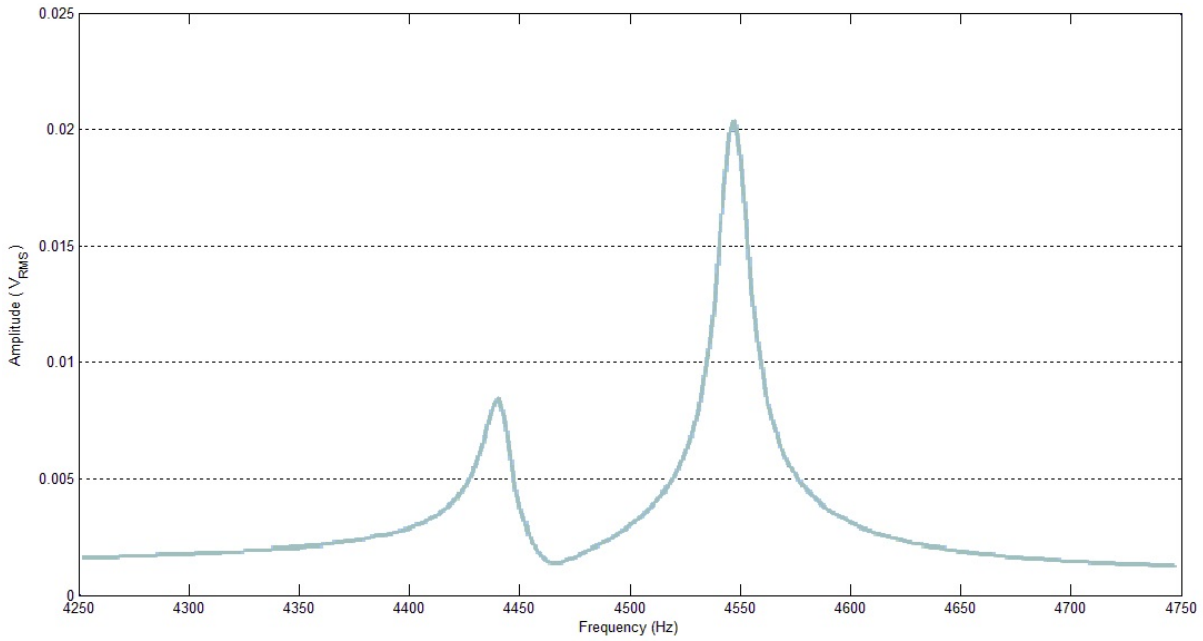

FIGURE 4.8: A frequency sweep of x-ray diffraction tube probe mounted on a chip.

This approach was abandoned, and small reflectors were attached the probes as is detailed in section 3.2.5 and shown in figure 4.11. Attaching this reflector only minimally lowers the resonance frequency due to the additional mass. The sum signal produced by this probe was an order of magnitude larger than previous tips. Although the signal could be reflected by the reflector, the probes still need to be coated with aluminum on one side. The photothermal laser did not excite any uncoated tips because the x-ray diffraction tubes are transparent allowing the blue laser light to pass through without much energy transferred to the probe.

When a frequency sweep, shown in figure 4.12 was performed on a probe with a reflector the V_{RMS} amplitude of the resonance peak at 3kHz was much greater and the Q factor of the peak was 400, a large increase over previous probes. Note that by the axis values of the frequency sweep, the amplitude was actually smaller. In actuality, the previous signals were amplified at higher gains. At the same photodiode gain as those previous scans this amplitude would saturate the electronics of the detection system. Note that the large increase in signal, and therefore the large difference in signal to noise ratio of the resonance peak may be attributed to the reflector. However, the fact that one of the resonance peaks grew while the other didn't must be attributed to probe mechanics. Whether this was produced by changes in the probe mounting rigidity, the reflector's large surface area acting to dampen motion in certain modes, or a small but effective change in the length of the tip after the bend is not clear.

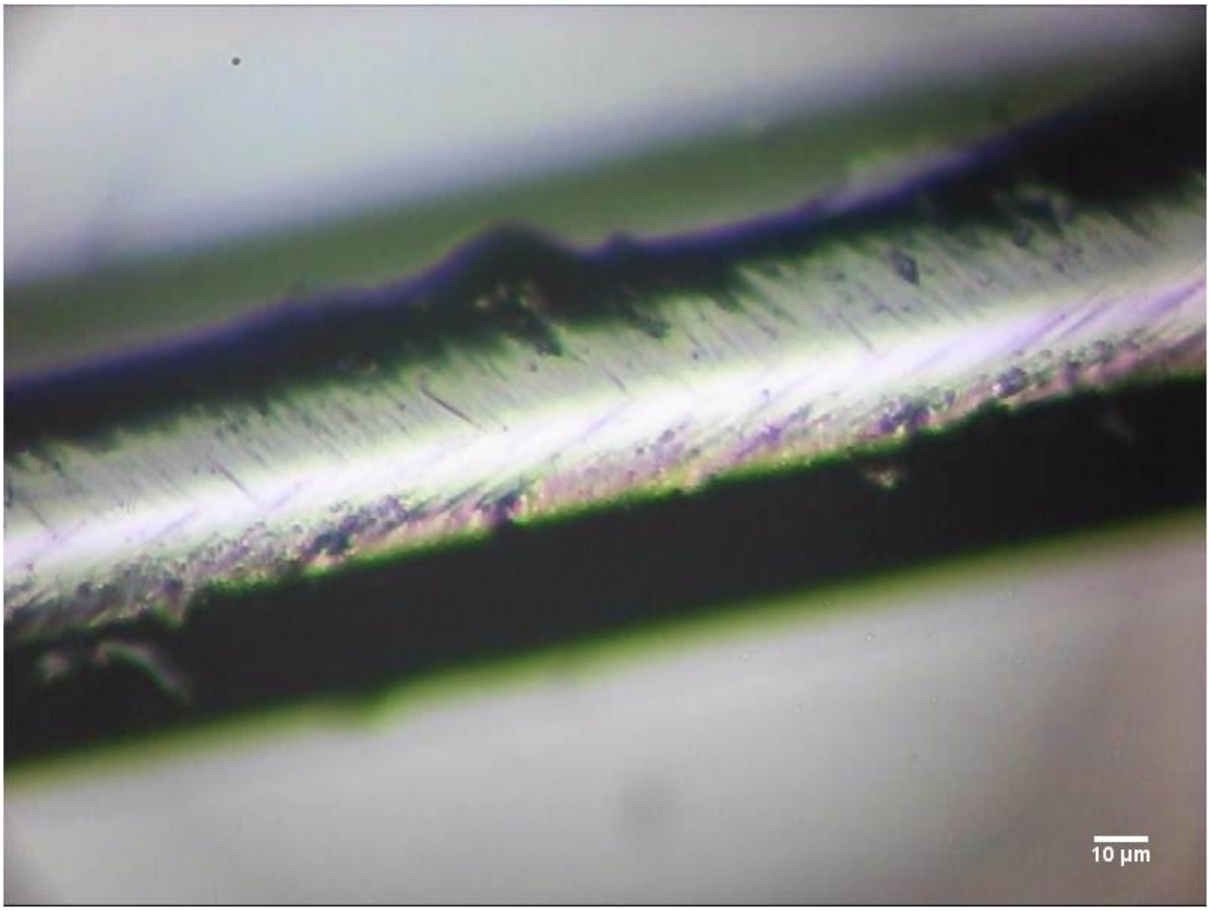

FIGURE 4.9: The scratches made through polishing this x-ray diffraction tube can be seen here. A coarse 5 micrometer grit polishing paper was used. The tube was marked by a black permanent marker previous to polishing so lighter areas have been polished.

Several AFM scans of a DVD sample were completed using this tip. One of this first scans is shown in figure 4.13. In this scan the pits are clearly visible, and the slope of the the walls of the pits can also be visualized with a minimum topographic height at the center of the pit. This means that the tip is able to resolve structures of half the diameter of one of the DVD pits which would be 160nm. These probes were tapered at the tip using the voltaic arc apparatus, a process described in 3.2.2. Measurements via the optical microscope determined that the tips were on the order of $10\mu m$ in diameter. The resolution of an AFM topography scan should be close to tip radius of the probe, so the two orders of magnitude difference in resolution versus tip size had to be investigated.

Another interesting feature of these probes was the quick degradation of resolution between successive scans. Using identical scan parameters over several scans resolution decreased for several tips. Shown in figure 4.14 is a larger topography scan taken of the

FIGURE 4.10: The scratches made through polishing this x-ray diffraction tube can be seen here. After the 5 micrometer grit polishing paper was used, progressively finer grits of polishing paper were used to smooth out the surface, although obtaining a smooth surface was not trivial.

DVD with the same scan parameters (aside from scan area size). Here the slope of the DVD pits cannot be seen, although the pit shapes may still be discerned.

To better understand these changes in resolution, Scanning Electron Microscopy (SEM) images of the tips were taken. Pictured in figure 4.15 is the tip of a probe. The tip is $6\mu m$ in diameter, close to the diameter measured using the optical microscope. It may be seen that tip of the cantilever, although unused, has some small features at the tip. This may be from handling or from the voltaic arc tapering process. An explanation for the high resolution initially observed in topography scans could be the tip interaction is actually occurring at one of these small features. These pieces of debris are loose, so they will fall off after some use, leading to the loss of resolution over several scans. A more robust tip is needed to perform reliable measurements; measurements should not rely on tips that quickly change in resolution. So, smaller tip size is required to perform consistent measurements of the quality already achieved.

Of the many tip images taken using the SEM, it became clear that the tapering of the probes produced a variety of tip shapes. This lack of reproducibility in tip shape is a clear indication of the need of a more rigorous tapering technique.

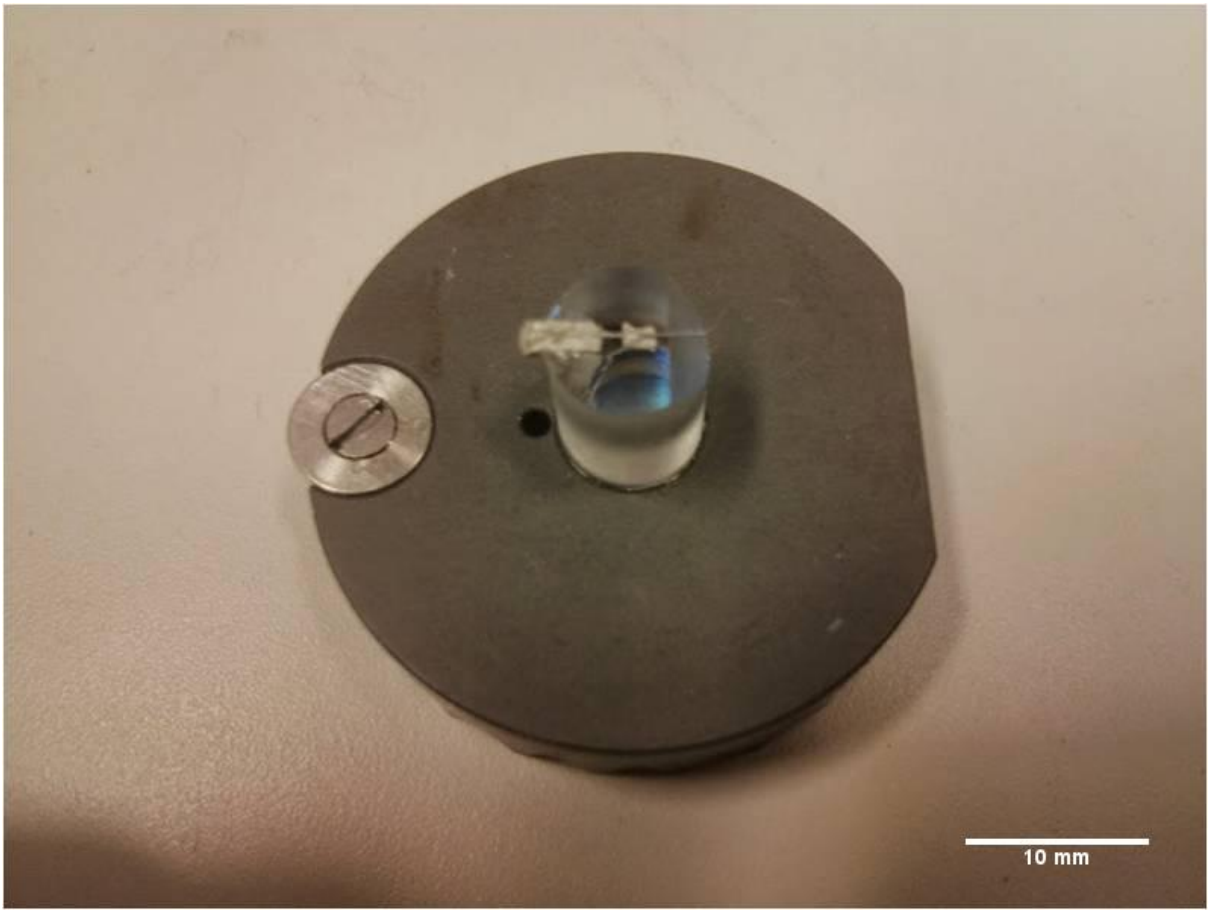

FIGURE 4.11: The reflector is mounted at the middle of the optical rod, to the right of the chip in this image.

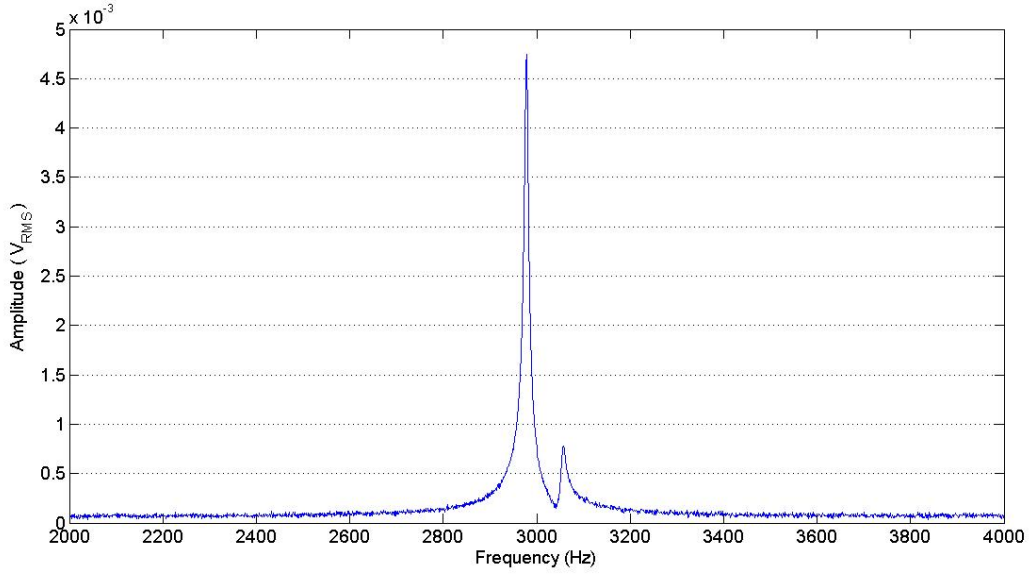

FIGURE 4.12: This frequency scan of a x-ray diffraction tube probe with a reflector has a resonance peak at 3kHz with a Q-factor of 400.

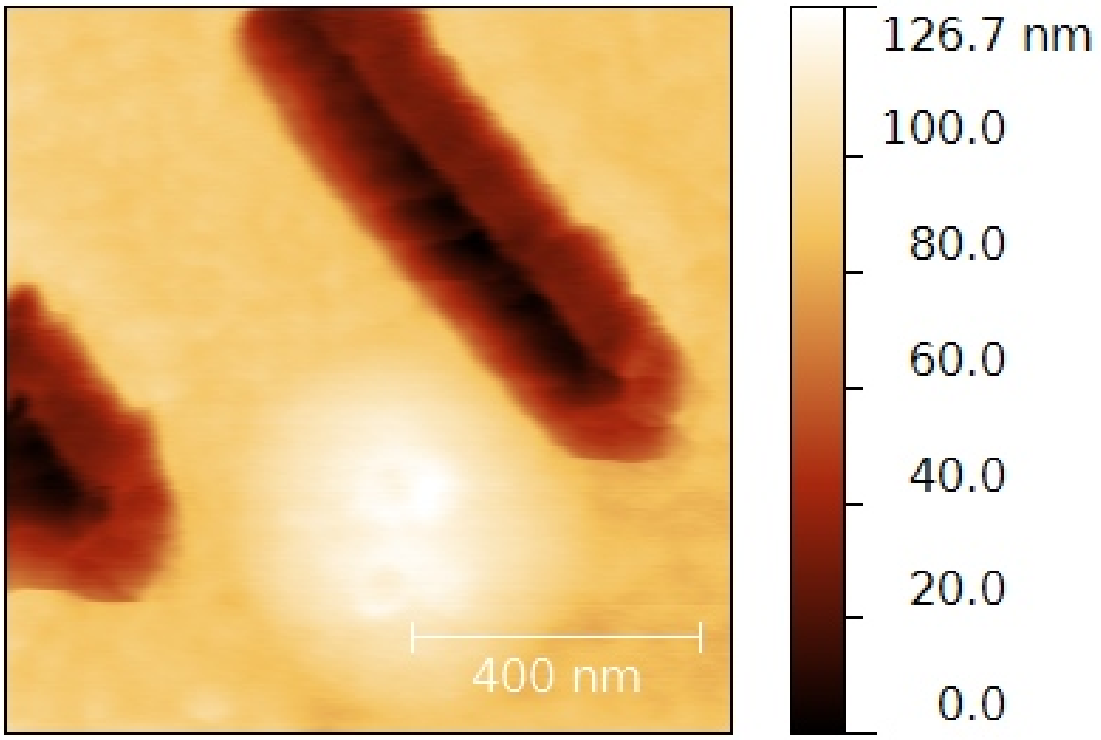

FIGURE 4.13: A topography scan of DVD pits of 320nm in diameter. The slope of the DVD pits seems to be evident, as well as a minimum in topography in the middle of the pit.

Another issue answered by this image pertains to the tip opening of these probes. A clear opening remains at the tip meaning that the tapering process leaves these tubes open which is required for future SICM measurements.

Despite these issues, the overall outcome was positive. Pipette probes may be used to perform topographic scans with high resolution, and they should be able to pass an ionic current. However, x-ray diffraction tubes have been shown to be less than ideal. An early experiment of trying to taper these tubes with a pipette puller resulted in no success. The fragility of the tubes prevented them being held and pulled firmly in a commercial pipette puller. So, while these tubes have demonstrated that pipettes probes are viable, a different glass tubing is required to undergo the pipette pulling process necessary to create sharp tips.

A final experiment was performed with these probes. Since SICM measurements are performed in electrolyte, these tips must operate in a liquid environment. One of the probes was excited to its resonance frequency, then lowered into liquid. A frequency sweep

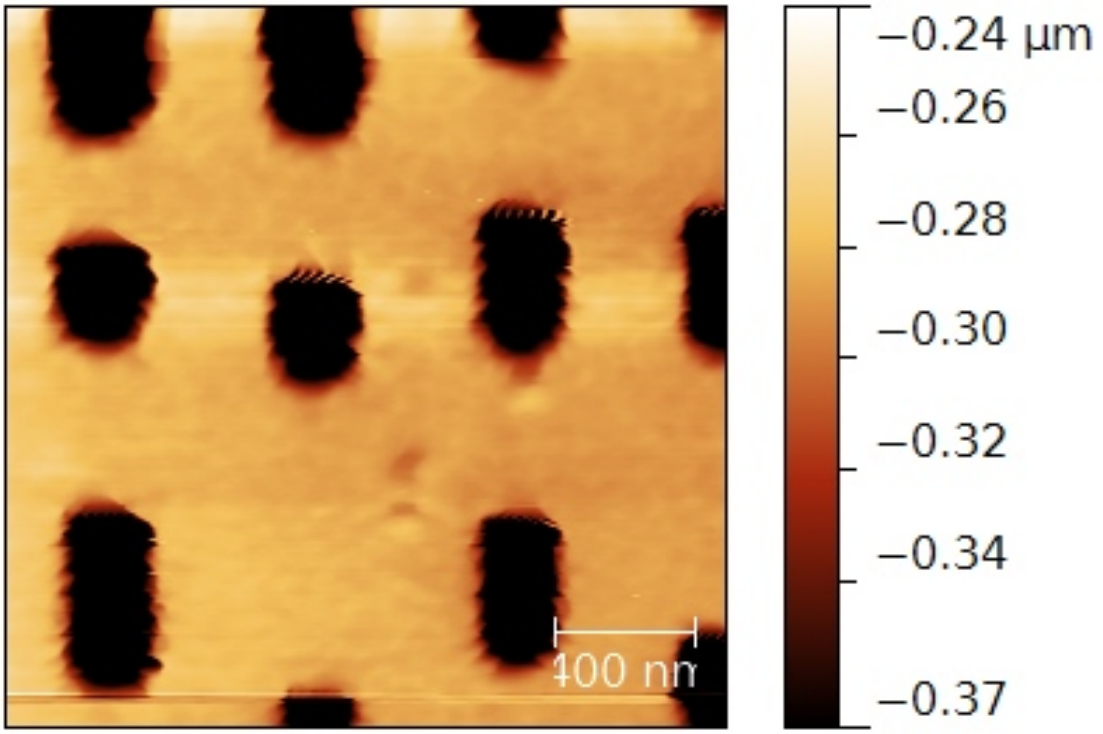

FIGURE 4.14: A topography scan of DVD pits of 320nm in diameter. The slope of the DVD pits cannot be seen in this iteration. The same tip was used to complete this scan, but this scan occurred after several more scans.

of the probe was taken when a decrease in oscillation amplitude occurred. As shown in figure 4.16 the amplitude of the resonance peak was dampened greatly to produce a low Q factor peak. While a decrease in excitation amplitude is expected, this decrease is drastic. It is a good indication of performance so see that the cantilever may still be excited in liquid, however a much sharper tip will have much less interaction with the liquid and will lessen this damping effect of the liquid. Plus, the electrolyte which will be used in the proposed experiments will be non-polar, which will decrease the hydrophyllic interaction which can be seen to occur as the tip enters the water.

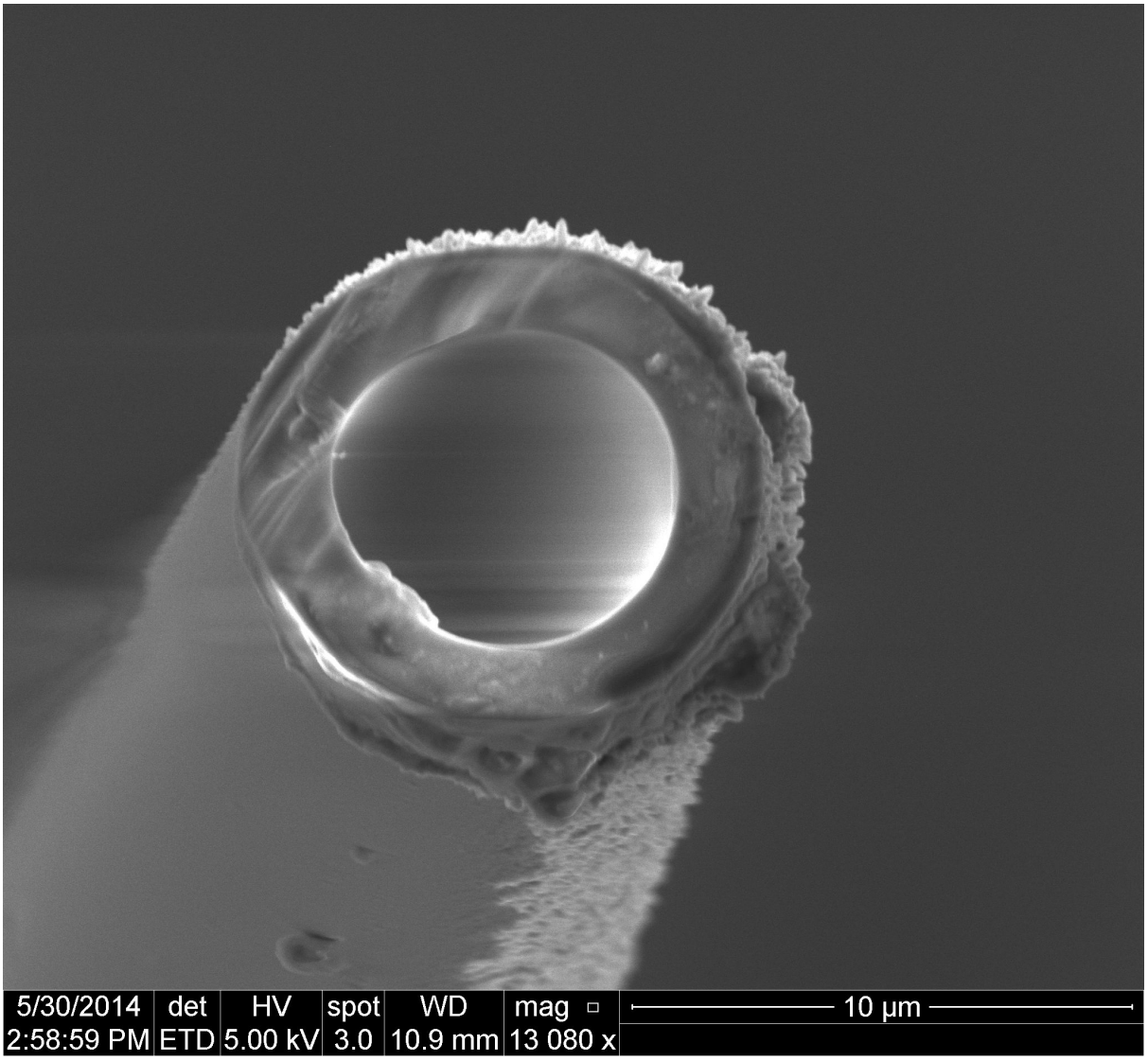

FIGURE 4.15: An x-ray diffraction probe tip is pictured. The grainy features on the right side of the probe are grains of deposited aluminum.

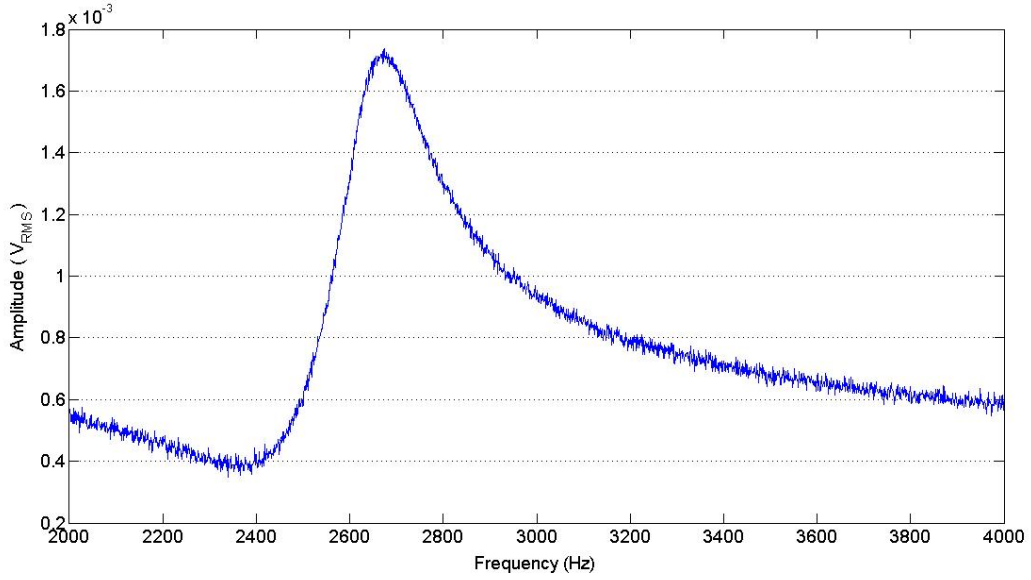

FIGURE 4.16: A frequency sweep of a cantilever with a tip immersed in water. The amplitude of oscillation decreases by over an order of magnitude as the tip transitions from air to liquid.

Chapter 5

Probe Fabrication Beginning with Capillary Tubes

5.1 Transfer of Knowledge from Previous Probes

Though the x-ray diffraction tube probes had to be abandoned, the knowledge gained by their creation should transfer directly to the new probes. Aluminum coatings for photothermal excitation, mounting of probes in a chip, and the general form of the tips are all shown to work in obtaining topographic data. Also, glass pulling and bending has been shown to leave an open channel for liquid. Also, the objectives of new probes are clear. The new probes must have similar mechanical properties to the glass borosilicate x-ray diffraction tubes, but the pipette pulling process must be different. A reproducible method for creating tapers pipette lengths on the order on millimeters must be established. This method must be reproducible and create well defined geometry at the taper and the tip. Furthermore the tip must be reduced in diameter as much as is possible without closing the end of the probe.

5.2 Pipette Cookbook

Although borosilicate capillaries commonly used by pipette pullers were initially considered at the outset of this project as the probes of choice, x-ray diffraction tubes seemed to be a better choice. A probe of varying diameter will have a much different stiffness constant at the base versus the tip. So, to be useful, pipettes with a sharp tip, followed by

FIGURE 5.1: An intracellular microelectrode pulled pipette fabricated from standard or thick walled 1.0mm x 0.5mm glass. The tip is 0.06μm and the taper is 12mm. The magnification of the image is 400x. [33]

a tapered region which slowly increases in diameter over a few millimeters is required. In original experimentation this was considerably more difficult than using x-ray diffraction tubes.

However, a manual produced by Sutter Instrument called the 'Pipette Cookbook' includes recipes for pulled pipettes of such dimensions [34]. Many of these recipes were used within the labs, and the parameters provided in the manual were varied slightly to produce optimal pipettes. One of the most promising recipes is the 'Intracellular Microelectrode' pulled pipette. The manual states that these probes, shown in figure 5.1 may have tips as small as 0.06μm with a taper of 12mm.

5.3 Lab Made Pipettes

Using the pipette cookbook as a reference, many recipes were followed. An issue with the creation of very thin long pipettes is stiffness. As seen in figure 5.2 the pipette can be seen to curl at the end. Taking this image was difficult due to the size of the tip. The small size required a high magnification and an exposure time of 200ms. Over that timescale the tip was rarely stationary. The flexible end of the pipette was frequently being moved from one side of the microscope view pictured in 5.2 by small air currents. The tip was not fixed to the microscope slide to avoid breaking this fragile glass. Also, the flexibility was greatest at the end of the glass pipette, so the most effective way to hold the pipette in place would be to affix it near within the micrometer thick region.

This flimsy pipette demonstrates the tapering issue. A sharp tip is required, but it must expand quickly to micrometer size or else the tip will be too flimsy to be used in AFM measurements.

Recipes for such tips were developed using a P-87 pipette puller from the Sutter recipes (note that the recipes found in the manual are specific to the P-97 and P-1000 pipette pullers). Shown in figures 5.3 and 5.4 is one of those tips. The diameter is less than

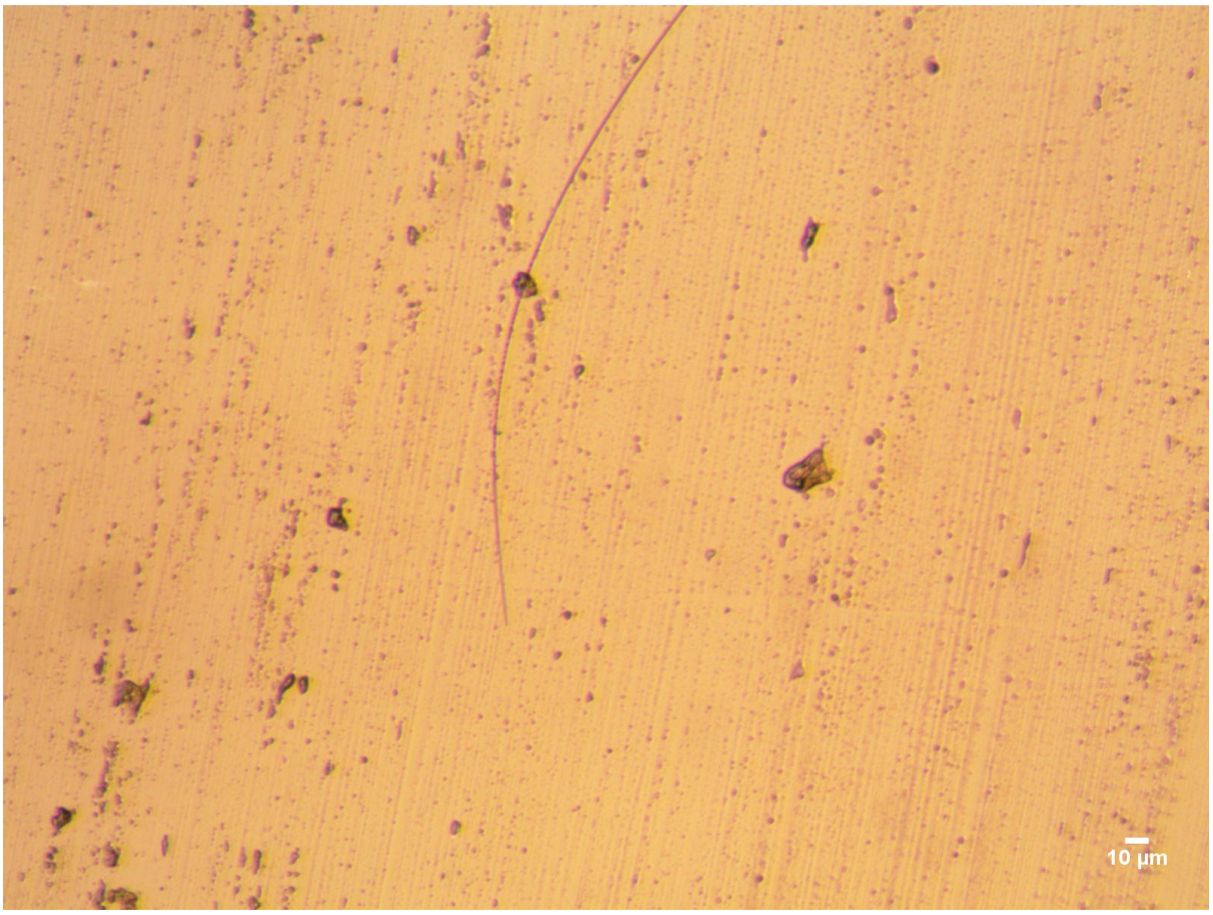

FIGURE 5.2: This pulled pipette is 1.5μm in diameter at the tip. The low stiffness at the tip allows the tip to be blown by small air drafts, this optical image was one of a series of blurred images.

500nm, it quickly widens to 10μm then tapers slowly over the next 400μm. This is exactly the pipette required to make probes, and will be used going forward.

5.3.1 Analysis

The same resonance frequency and stiffness calculations which were successful in predicting the characteristics of the x-ray diffraction tube probes were used for these pipettes. A probe with a length of 400μm made of the pipette pictured in figure 5.3 will have a stiffness of 5N/m and a resonance frequency of 6635Hz.

Probes have been produced of this size. These pipettes are expected (and known from patch clamp measurements) to have smooth tips as they get heated. The x-ray tubes fracture at the tip, hence their rough appearance in SEM imaging. SEM imaging will

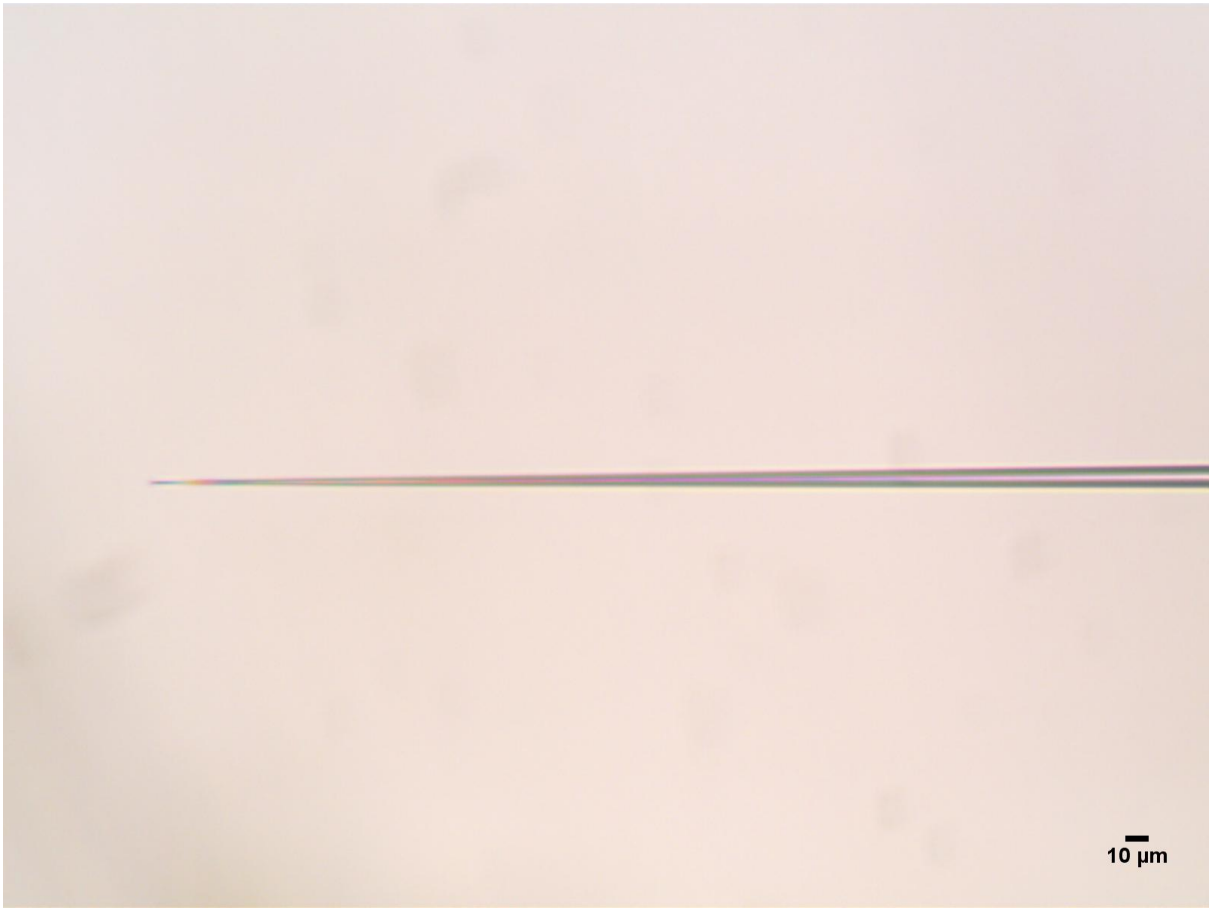

FIGURE 5.3: This pulled pipette is less than $0.5\mu m$ in diameter at the tip. The tip expands to $10\mu m$ quickly then tapers slowly over the next $400\mu m$.

also determine exactly the diameter of these tips, which is quoted to be in the range of 30nm according to the Pipette Cookbook.

Currently issues of reflector size are being dealt with. Smaller reflectors are required for this tip in order to not dampen the movement of the probe. An option is use silicon AFM cantilevers as reflectors, a method that we have explored and has been used to generate increased signals. Regardless, a probe of this size has been created, and the steps leading to topographic imaging using this probe have already been demonstrated in the previous experiments on x-ray diffraction tubes.

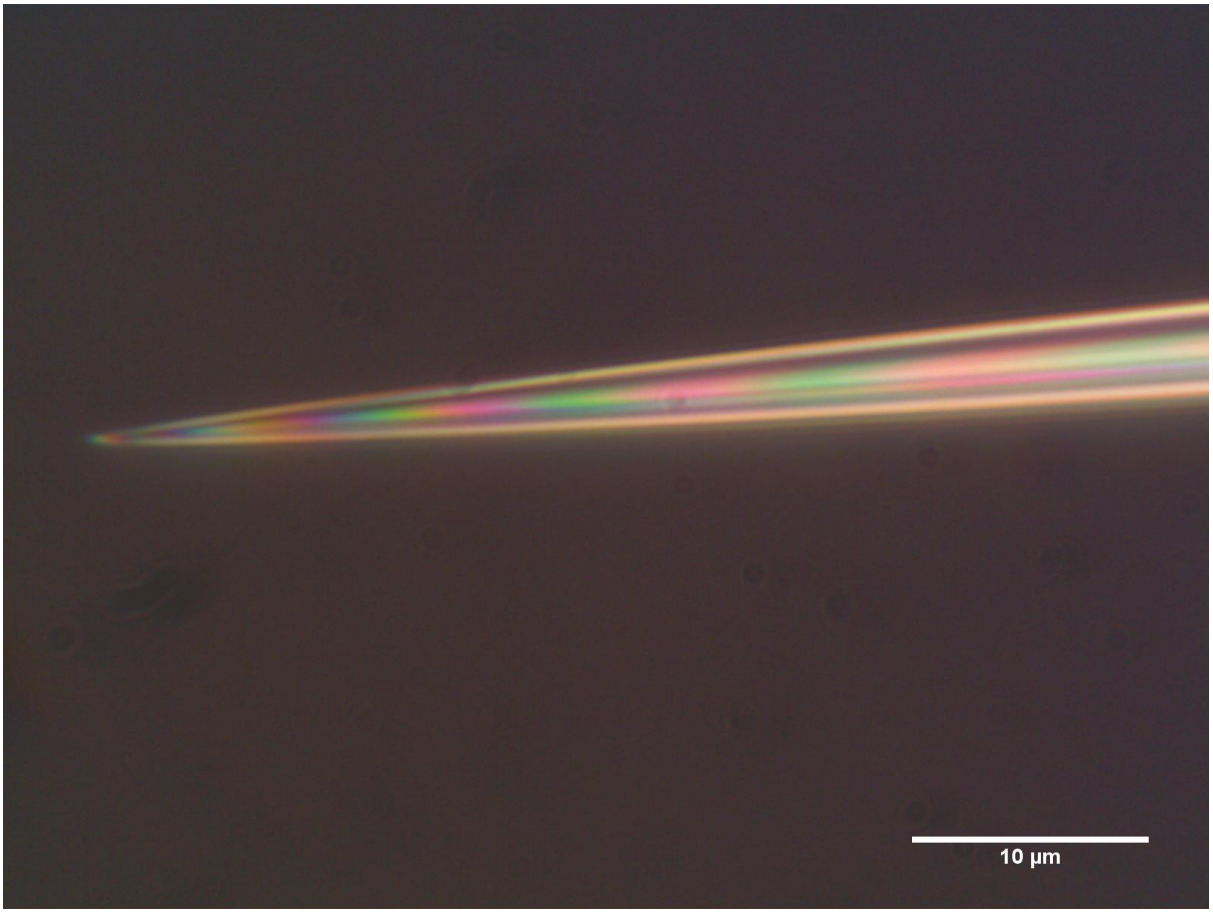

FIGURE 5.4: This view at 10x higher magnification shows the sharpness of the tip.

Chapter 6

Conclusions and Future Direction

In this study the viability of tips for use both in Scanning Ion Conductance Microscopy (SICM) measurements and Atomic Force Microscopy (AFM) measurements in an integrated SICM-AFM system intended for study of lithium ion battery charging characteristics was examined and many probes were fabricated. Capillary tubes were bent by voltaic arc to demonstrate that hollow pipettes could be formed into the shape of an AFM cantilever which could be used within the Electrochemical Atomic Force Microscope which was used to do all AFM measurements (frequency sweeps, topographic scans, etc.). Then x-ray diffraction tubes were bent in the same shape and an aluminum coating was applied to increase the intensity of reflected light from the incoming detection laser to the photodiode. A topographic scan of a DVD surface showing periodic unknown features and a frequency sweep featuring two adjacent resonance peaks indicated the need for a more rigid probe holder. The probe was mounted in a V-groove micromachined into a silicon chip on the AFM head optical rod, the tip was shortened, and the cantilever portion of the pipette was made to be 5mm in length to test calculations which predicted this would produce a resonance frequency of 4095Hz at a stiffness that would allow tapping mode measurements. A frequency sweep was performed with this cantilever which demonstrated a separation in the two resonance peaks previously seen and a resonance frequency of 4545Hz which was quite close to the predicted value seeing as the calculation was for an ideal cylindrical cantilever without a tip as this probe had. To improve the overall signal reflected by the curved surface of the x-ray diffraction probe an attempt to polish the probe surface was attempted with poor results. Instead, an aluminum coated glass reflector was mounted on a probe and this probe exhibited a greatly increased amount of reflected laser light. It had a resonance peak of 3kHz and a Q factor of 400 and was nearly

10 times the amplitude of the secondary resonance peak that often appears in these cantilevers. Topographic scans of DVD pits were performed with these probes to determine that in the first few scans the probes had resolutions of better than 160nm, but quickly decreased to resolutions closer to 300nm. The tips were examined by Scanning Electron Microscopy (SEM) and it was hypothesized that small unstable features on the tip end surface were responsible for the high resolution. Also, the SEM images demonstrated that these tips remain open through the tapering process which is crucial for the ionic flow which must pass through the tip during SICM measurements. The ability of these tips to perform high resolution measurements initially, the non-uniform but open tips created by the voltaic arc tapering method, and the large amplitude damping of the probe in water lead to the conclusion that while pipette cantilevers can be used for topography and this geometry can probably be used for SICM measurements, x-ray diffraction tubes could not be pulled into sharp and reproducible enough pipettes. Work was done to create borosilicate pipettes using a pipette puller which have a tip size of 25nm which widens of approximately $10\mu m$ for a length of $400\mu m$, and calculations predict that these probes will have similar resonance frequencies and stiffness constants as the x-ray diffraction tubes which were shown to be capable of producing topography. This study has clearly demonstrated that pipette tips can be used as AFM tips, has determined a method of probe production to do this, and has created by pipettes which are calculated to have usable stiffness constant and resonance frequency, and a topographic resolution on the order of 25nm.

As this project is continued, there are some essential steps to take before lithium ion batteries can be measured. First, new smaller reflectors must be created to fit on these new borosilicate capillary based pulled pipettes. With this done the predicted resonance frequency and stiffness must be tested. With this done topography can once again be tested. Though the tip size of these cantilevers will allow for topographic resolution on the order of 25nm, better resolution is required. Focused Ion Beam deposition can be used to deposit a thin platinum wire on the tip of the probe. The size of the wire will determine resolution, and this should be on the order of 1nm, which would acceptable for topographic resolution in studying lithium ion batteries. Once topography in air is accomplished, the same should be done in liquid. With topography firmly established an electrode may be introduced into the probe and SICM measurements on patterned gold surfaces may be done to calibrate and test the resolution of this probe. Interestingly, SICM probes are said to have tip openings between 30nm and 100nm. The outside diameter of the current pipettes is estimated from the cookbook to be 30nm. An empirical observation made during the tapering of many fibers is that when a capillary is pulled

into a pipette the ratio of inner radius to outer radius usually stays constant. This tip opening observation needs to be confirmed with SEM, but if it holds true then the opening could be as small as 15nm. Since resolution of SICM measurements is directly related to tip openings diameter, resolution could be 2 times higher than other probes. Additionally, since the probe will also be able to detect topography via AFM tapping mode, tip crashing will be prevented by detecting large changes in topographic height. As such SICM measurement may be performed closer to sample surfaces which will also increase conduction measurement resolution. If these hypotheses are proven correct then this integrated SICM-AFM system could produce conduction measurements with higher resolution than most SICM systems within the literature.

Appendix A

Electrochemical Atomic Force Microscope

FIGURE A.1: The AFM used in this study without the photothermal attachment and a silicon cantilever holder.[24]

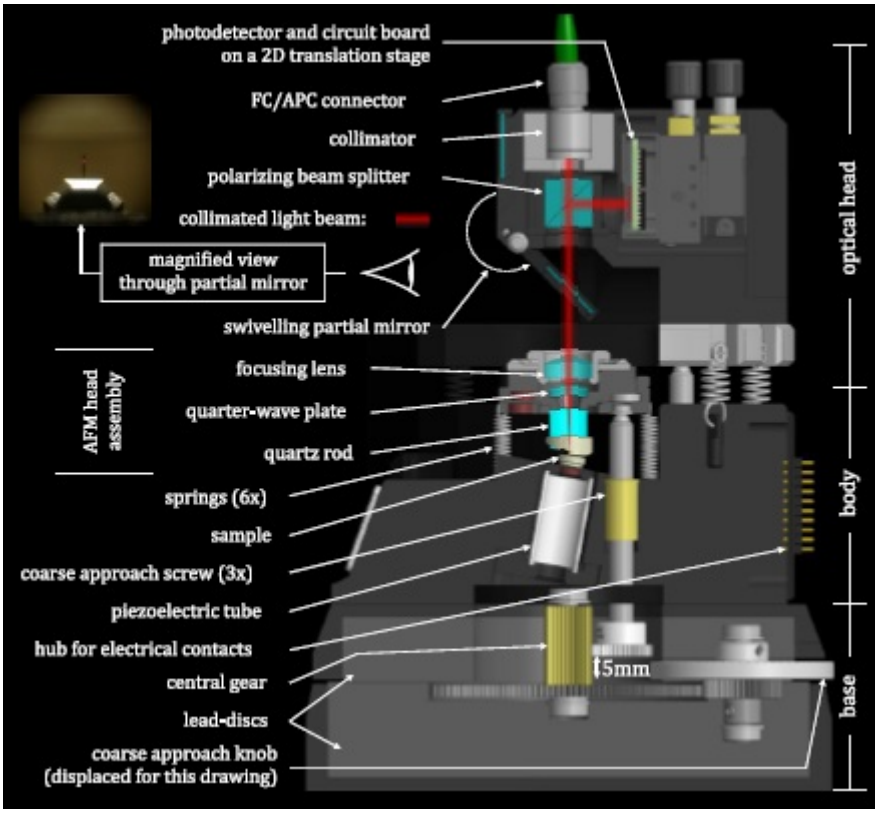

FIGURE A.2: A technical side view drawing of the electrochemical AFM used in this study without the photothermal attachment. [24]

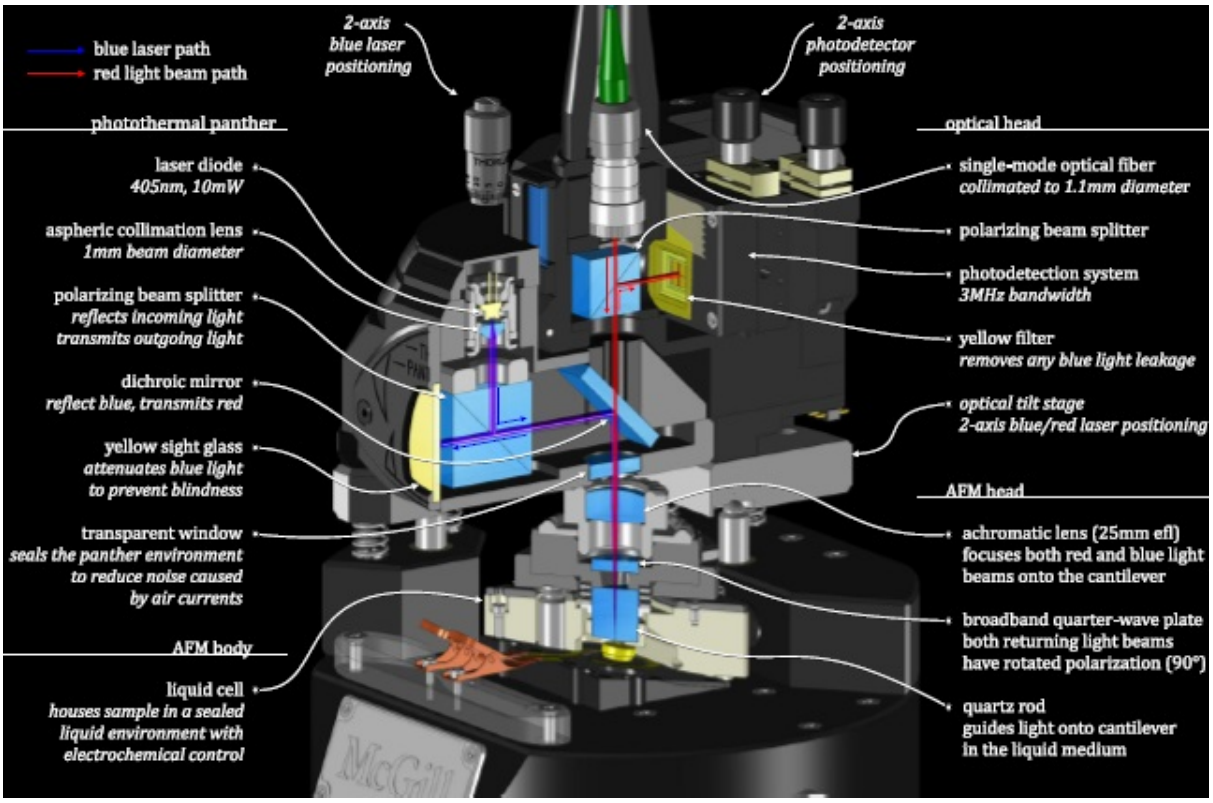

FIGURE A.3: A technical side view drawing of the electrochemical AFM used in this study with the photothermal attachment [24]

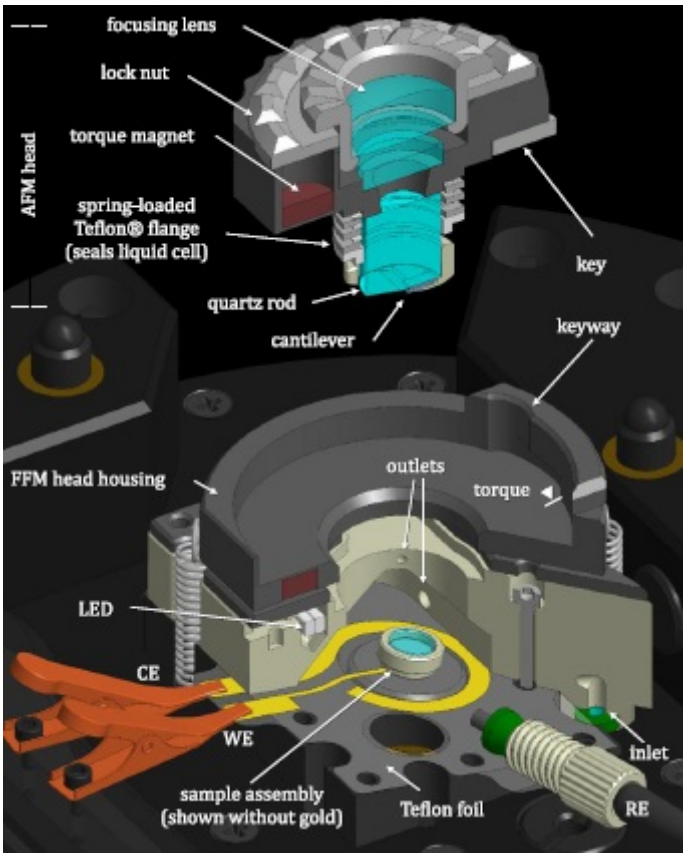

FIGURE A.4: A technical side view drawing of the electrochemical cell used within the ECAFM with silicon cantilever holder [24]

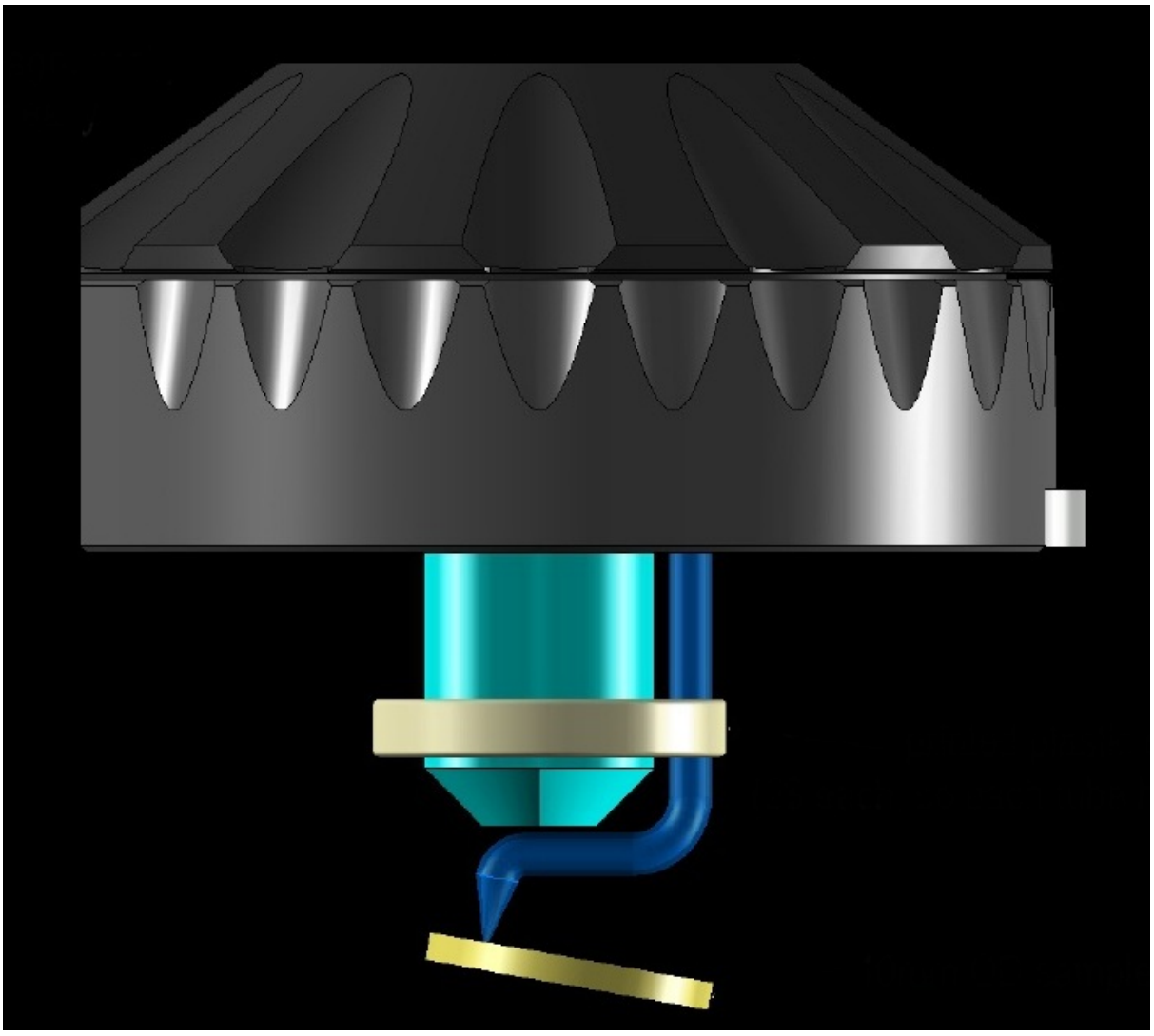

FIGURE A.5: A technical side view drawing of the ECAFM head with silicon cantilever holder. This design and drawing was completed by Aleks Labuda.

Bibliography

[1] Harrop P.; Das R. Car traction batteries - the new gold rush 2010-2020. *IDTechEx Research Reports*, 2010. URL http://www.idtechex.com/research/reports/car_traction_batteries_the_new_gold_rush_2010_2020_000232.asp.

[2] Hoppmann J.; Hoffmann V.H. The economic viability of battery storage for residential solar photovoltaic systems – a review and a simulation model. *Paper forthcoming in Renewable & Sustainable Energy Reviews*, 2014. URL http://www.sustec.ethz.ch/people/jhoppmann/Hoppmann_et_al__The_Economic_Viability_of_Battery_Storage_for_Residential_Solar_Photovoltaic_Systems_-_A_Review_and_a_Simulation_Model.pdf.

[3] Energy storage: Packing some power. *The Economist*, March 2012. URL http://www.economist.com/node/21548495?frsc=dg%7Ca.

[4] U.S. Department of Energy. Grid energy storage. December 2013. URL http://energy.gov/sites/prod/files/2013/12/f5/Grid%20Energy%20Storage%20December%202013.pdf.

[5] Electric Power Research Institute. Electrical energy storage technology options. *Report 1020676*, December 2010.

[6] Dunn B.; Kamath H.; Tarascon J.M. Electrical energy storage for the grid: A battery of choices. *Science*, (334):928–935, 2011. URL http://www.sciencemag.org/content/334/6058/928.full.html.

[7] Mandel J. Doe promotes pumped hydro as option for renewable power storage. *New York Times*, October 2010. URL http://www.nytimes.com/gwire/2010/10/15/15greenwire-doe-promotes-pumped-hydro-as-option-for-renewa-51805.html?pagewanted=all.

[8] Etacheri V. Challenges in the development of advanced li-ion batteries: a review. *Energy & Environmental Science*, 4:3243, July 2011.

[9] Berman B. *New York Times*, The Battery-Driven Car Just Got a Lot More Normal, May 2012. URL http://www.nytimes.com/2012/05/06/automobiles/autoreviews/the-battery-driven-car-just-got-a-lot-more-normal.html?_r=2&ref=automobiles&.

[10] Huilong F.; Zhiwei P.; Lei L.; Yang Y.; Wei L.; Errol L.; Xiujun F.; James T. Preparation of carbon-coated iron oxide nanoparticles dispersed on graphene sheets and applications as advanced anode materials for lithium-ion batteries. *Nano Research*, 7(4):1–9, 2014. ISSN 1998-0124. doi: 10.1007/s12274-014-0416-0. URL http://dx.doi.org/10.1007/s12274-014-0416-0.

[11] Wang Y.; He P.; Zhou H. Olivine lifepo4: development and future. *Energy Environ. Sci.*, 4:805–817, 2011. doi: 10.1039/C0EE00176G. URL http://dx.doi.org/10.1039/C0EE00176G.

[12] Newman J.; Thomas K. E.; Hafezi H.; Wheeler D.R. Modeling of lithium-ion batteries. *Journal of Power Sources*, 119–121(0):838 – 843, 2003. ISSN 0378-7753. doi: http://dx.doi.org/10.1016/S0378-7753(03)00282-9. URL http://www.sciencedirect.com/science/article/pii/S0378775303002829. Selected papers presented at the 11th International Meeting on Lithium Batteries.

[13] Srinivasan V.; Newman J. Discharge model for the lithium iron-phosphate electrode. *Journal of The Electrochemical Society*, 151(10):A1517–A1529, 2004. doi: 10.1149/1.1785012. URL http://jes.ecsdl.org/content/151/10/A1517.abstract.

[14] Morgan D.; Van der Ven A.; Ceder G. Li conductivity in lixmpo4 (m = mn, fe, co, ni) olivine materials. *Electrochemical And Solid State Letters*, 7(2):A30, 2004.

[15] Delmas C.; Maccario M.; Croguennec K.; Ke Cras F.; Weill F. Lithium deintercalation in $LiFePO_4$ nanoparticles via a domino-cascade model. *Nature Materials*, 151 (7):665–671, July 2008. URL http://www.nature.com/nmat/journal/v7/n8/abs/nmat2230.html.

[16] C. Ramana, A. Mauger, F. Gendron, C. Julien, and K. Zaghib. Study of the li-insertion/extraction process in $LiFePO_4/PO_4$ nanoparticles via a domino-cascade model. *Journal of Power Sources*, 187(2):555–564, February 2009. URL http://www.sciencedirect.com/science/article/pii/S0378775308021794.

[17] Harris S.; Timmons A.; Baker D.; Monroe C. Direct in situ measurements of li transport in li-ion battery negative electrodes. *Chemical Physical Letters*, 485(4-6):

265–274, January 2010. URL http://www.sciencedirect.com/science/article/pii/S0009261409015462.

[18] L. Laffont, C. Delacourt, P. Gibot, M. Yue Wu, P. Kooyman, C. Masquelier, and J. Marie Tarascon. Study of the lifepo4/fepo4 two-phase system by high-resolution electron energy loss spectroscopy. *Chemistry of Materials*, 18(23):5520–5529, 2006. doi: 10.1021/cm0617182. URL http://pubs.acs.org/doi/abs/10.1021/cm0617182.

[19] W. C. Chueh, F. El Gabaly, J. D. Sugar, N. C. Bartelt, A. H. McDaniel, K. R. Fenton, K. R. Zavadil, T. Tyliszczak, W. Lai, and K. F. McCarty. Intercalation pathway in many-particle $LiFePO_4$ electrode revealed by nanoscale state-of-charge mapping. *Nano Letters*, 13(3):866–872, 2013. doi: 10.1021/nl3031899. URL http://pubs.acs.org/doi/abs/10.1021/nl3031899.

[20] Al Hallaj S; Maleki H; Hong J.S.; Selman R.J. Thermal modeling and design considerations of lithium-ion batteries. *Journal of Power Sources*, 83(1):1–8, 1999.

[21] B. Bhusan and H. (Eds) Fuchs. *Applied Scanning Probe Methods II: Scanning Probe Microscopy Techniques*. Nanoscience and Technology. Springer, 2006.

[22] SPM training guide: Atomic Force Microscopy (AFM). http://www.nanophys.kth.se/nanophys/facilities/nfl/afm/fast-scan/bruker-help/Content/SPM%20Training%20Guide/Atomic%20Force%20Microscopy%20(AFM)/Atomic%20Force%20Microscopy%20(AFM).htm. Accessed: 2014-07-22.

[23] yashvant http://kristian.molhave.dk. Afmsetup. URL http://commons.wikimedia.org/wiki/File:AFMsetup.jpg#mediaviewer/File:AFMsetup.jpg. Accessed: 2014-07-23.

[24] Labuda A. Adventures in atomic force microscopy: towards the study of the solid-liquid interface, August 2012. URL http://alekslabuda.com/sites/default/files/aleks_labuda_phd_thesis.pdf.

[25] Hong-Qiang L. The common AFM modes. URL http://www.chembio.uoguelph.ca/educmat/chm729/afm/details.htm. Accessed: 2014-07-23.

[26] Eaton P.; West P. *Atomic Force Microscopy*. Oxford University Press, Great Clarendon Street, Oxford OX2 6DP, 2010.

[27] Fang F.Z.; Xu Z.W.; Dong S. Study on phase images of a carbon nanotube probe in atomic force microscopy. *Measurement Science and Technology*, 19(5):055501, 2008. URL http://stacks.iop.org/0957-0233/19/i=5/a=055501.

[28] Happel P.; Thatenhorst D.; Dietzel I.D. Scanning ion conductance microscopy for studying biological samples. *Sensors*, 12(11):14983–15008, 2012. ISSN 1424-8220. doi: 10.3390/s121114983. URL http://www.mdpi.com/1424-8220/12/11/14983.

[29] Pellegrino M.; Orsini P.; Pellegrini M.; Baschieri P.; Dinelli F.; Petracchi D.; Tognoni E.; Ascoli C. Weak hydrostatic forces in far-scanning ion conductance microscopy used to guide neuronal growth cones. *Neuroscience Research*, 69(3):234 – 240, 2011. ISSN 0168-0102. doi: http://dx.doi.org/10.1016/j.neures.2010.11.009. URL http://www.sciencedirect.com/science/article/pii/S0168010210028543.

[30] Schäffer T. E.; Ionescu-Zanetti C.; Proksch R.; Fritz M.; Walters D. A.; Almqvist N.; Zaremba C. M.; Belcher A. M.; Smith B. L.; Stucky G. D.; Morse D. E.; Hansma P. K. Does abalone nacre form by heteroepitaxial nucleation or by growth through mineral bridges? *Chemistry of Materials*, 9(8):1731–1740, 1997. doi: 10.1021/cm960429i. URL http://pubs.acs.org/doi/abs/10.1021/cm960429i.

[31] Young W.C.; Budynas R.G. *Roark's Formulas for Stress and Strain*. McGraw-Hill, New York, NY, 7 edition, 2002.

[32] Wikipedia. List of area moments of inertia — Wikipedia, the free encyclopedia, 2014. URL http://en.wikipedia.org/wiki/List_of_area_moments_of_inertia#cite_note-1. [Online; accessed 28-July-2014].

[33] Juvinal R. and Marshek K. *Fundamentals of Machine Component Design*. John Wiley, 4 edition, 2006.

[34] Oesterle A. *P-1000 & P-97 Pipette Cookbook*. Sutter Instruments, Rev. G edition, 2011.